MINISTRY OF AVIATION

AERONAUTICAL RESEARCH COUNCIL

CURRENT PAPERS

Wall Interference at Transonic Speeds on a Hemisphere-Cylinder Model.

by

E. W. E. Rogers, M.Sc.,
and
I. M. Hall, Ph.D.
of the Aerodynamics Division, N.P.L.

Wall Interference at Transonic Speeds
on a Hemisphere-Cylinder Model
- By -
E. W. E. Rogers, M.Sc., and
I. M. Hall, Ph.D.
of the Aerodynamics Division, N.P.L.

25th September, 1959

SUMMARY

Tests have been made in three N.P.L. wind tunnels on a
pressure-plotting model consisting of a long cylinder with a
hemispherical nose. The surface pressure distributions were measured
for stream Mach numbers between 0.7 and 1.1 at zero model incidence,
and schlieren photographs were taken. The blockage ratios were
0.211%, 0.117% and 0.120%.

The principal feature of the flow is the effect of working
section size on the rate at which the terminal shock wave moves back
along the model with increasing stream Mach number. This is thought
to depend mainly on the distance from the model to the slotted walls
of the tunnel, and not necessarily on the blockage ratio. The distance
of the solid sidewall is important in influencing the local Mach number
ahead of the terminal shock, by reflecting the expansion-wave system
originating near the model nose.

CONTENTS

1. Introduction

Recently there has been an increased interest in the interference effects experienced by models tested at transonic speeds in ventilated tunnels. In part, this has arisen from a clearer understanding of the flow problems involved, as a result of careful experimental studies; at the same time, transonic theory has progressed to a stage where the possible nature and magnitude of interference effects can sometimes be predicted.

One particular interference phenomenon which has occasioned interest is the reduced rate of terminal shock movement with stream Mach number on a long or semi-infinite body as the model blockage rate is increased. This effect seems to have been noticed initially by Roe[1] in the United Kingdom and by Page[3] in the U.S.A., and is of obvious importance in assessing the validity of wind-tunnel measurements, particularly of static pressure.

In an earlier report by the present authors[2] this delay in shock movement was shown to exist even when the model blockage ratio was as low as 0.0021%, the effect increasing markedly as the blockage ratio became greater. These tests were made with hemisphere-cylinder models* of different sizes in the N.P.L. 18 in. × 14 in. tunnel. The static pressure on these models could only be measured at a position some $8\frac{1}{2}$ diameters from the nose and the results obtained, although demonstrating the shock-delay phenomenon, were insufficiently detailed to enable the reasons for the effect to be assessed. Moreover, since the models had been tested in only one tunnel, it was not possible to determine whether the shape of the tunnel cross-section, in addition to the blockage ratio, was important.

In order to provide further information, tests on an additional hemisphere-cylinder model were made in three different transonic tunnels at the N.P.L. This model had pressure holes distributed around the nose and along the first 14 diameters of the body. The results, which were obtained in November and December, 1958, are described in the present report.

2. Experimental Details

2.1 The model

The model was that used for the supersonic experiments discussed in Ref.4. The main part of the body was cylindrical, of diameter 0.8 in., and made from a steel tube coated with araldite. Hyperdermic tubes were embedded in the latter and brought to the surface to form the pressure holes, which are spaced at intervals of 0.94 of the model diameter (d). The hemispherical head screws into the main body and contains a further seven pressure holes. The position of these, and those situated along the cylindrical portion, are given in Table 1.

2.2 The tunnels

The model was tested in three of the N.P.L. induced-flow wind tunnels. All have transonic working sections consisting of solid sidewalls (containing glass windows) and liners with longitudinal slots above and below the model. Each liner has ten equally-spaced slots and two slots of half the standard width at the side edges; one-eleventh of the tunnel width is open to the plenum chamber in each case.

Because/

---

*The largest model tested in Ref.2 was a full-size Mk IXA pitot-static head, which, because of the pitot orifice, does not have a completely hemispherical nose. This seems to have been unimportant.

Because of the need to provide adequate volume in the plenum chamber, the working-section height is less than that for subsonic or supersonic operation with solid liners. The relevant dimensions, together with the model blockage ratio (B) are given below.

Nominal size of working section	Actual size of working section	$B \left(= \dfrac{\text{model cross-sectional area}}{\text{working section area}} \right)$		
18 in. × 14 in.	17 in. × 14 in.	0.211 %		
36 in. × 14 in.	$30\frac{3}{4}$ in. × 14 in.	0.117%		
25 in. × 20 in.	21 in. × 20 in.	0.120%		

In the present text, the tunnel will be referred to by means of the actual, and not the nominal, size of the working section.

2.3 Experimental technique

In each tunnel the method of mounting the model was similar, it being held in a sleeve at the end of a side-support passing through a turntable in one of the solid sidewalls. The same support gear was used in the $30\frac{3}{4}$ in. × 14 in. and 21 in. × 20 in. tunnels, the upstream end of the sleeve being about 37d from the nose of the model. A slightly different side support was employed during the tests in the 17 in. × 14 in. tunnel, the distance from the model nose to the beginning of the sleeve being about 26.5d.

Pressure distributions were obtained with the model at zero incidence and these were supplemented by schlieren photographs. The nominal stream Mach number was deduced from the pressure at a hole on the central slat of one of slotted liners, at a position well upstream of the model nose. Observations were made at nominal Mach numbers between 0.7 and 1.10. Subsequently a correction was applied to allow for known differences between the nominal Mach number and that at the model position in the empty tunnel. The actual pressure gradients present in the working sections are small and it was considered sufficient to define the corrected stream Mach number (M_o) as that appropriate to a position midway along the model length. No corrections have been applied to the present results to allow theoretically for the effects of wall constraint on stream Mach number or local pressures.

All tests were run with a stream total pressure which was nearly atmospheric; the Reynolds number varied with stream Mach number and based on model diameter was 0.32×10^6 at $M_o = 1.00$.

3. Results

The complete set of pressure distributions for all three tunnels is given in Table 2, and some of these results are presented in graphical form in Fig.1. In both the Tables and the Figures, the observed local pressure (p) has been divided by the stream total pressure (H).

The development of the flow about a hemisphere-cylinder model has been discussed in detail in Ref.2 but it is perhaps worth recalling the main features. A local supersonic region forms close to the shoulder of the model just below $M_o = 0.70$, but a well-defined shock system is not obtained until nearly $M_o = 0.90$. This consists of a front inclined shock, originating from the vicinity of the shoulder and propagating through the local supersonic flow until it reaches the terminal shock. The latter is dish-shaped at stream Mach numbers below about 0.97 and thereafter is normal. At $M_o = 0.90$, the terminal shock is about $1\frac{1}{2}$ diameters from the nose of the model and the rearward movement is slow until the stream Mach number exceeds about 0.97. This is true even when the blockage ratio is very small.

The/

The subsequent movement of the terminal shock is clearly shown in the three parts of Fig.1, and it is apparent that the rate of movement is less when the blockage ratio is high.

A typical pressure distribution obtained at M_O = 1.050 in the 17 in. × 14 in. tunnel and showing the terminal shock at about 7.6d, together with the corresponding schlieren photograph, is included as Fig.2. The largest recompression is associated with the region between the shoulder and about 2 diameters and hence with the front inclined shock. The local surface Mach number ahead of the terminal shock is comparatively low (about 1.09) and behind the shock the pressure falls steadily to the free-stream value, this being achieved at about 12.5d. The final, small, rise in pressure may well be associated with the presence of the support sleeve downstream. The characteristic pressure distribution is therefore one which has a rapid expansion around the curved nose until the maximum local velocity is reached near the shoulder. A rapid compression is then followed by a region where the surface pressure changes only slowly, until the terminal shock is reached. The local Mach number is subsonic to the rear of this shock and the pressure then falls to the free-stream value.

At the higher test Mach numbers the reflections of the bow shock wave from the tunnel walls intersect the model and cause local pressure changes on its surface. Events of this type are labelled R_B on the pressure distributions, suffixed in some cases by either s or T to indicate that the reflection is from a solid or a slotted wall. The surface pressures are also modified by the reflections of the front inclined wave when these strike the model. Such reflections are denoted by R_F with the same system of suffices as for the bow wave.

At somewhat lower stream Mach numbers, the reflected front inclined shock intersects the terminal shock at a position between the model and the wall (as in Fig.2). This must imply some modification of the terminal shock itself, but for the present report the term has been retained for the final normal shock wave in the flow about the model.

3.1 Terminal shock position and movement

The position of the terminal shock is most conveniently found by measuring the schlieren photographs. The results obtained from the three tunnels are shown in Fig.4, which also suggests that these measurements can be supplemented with sufficient accuracy by using the position* of the appropriate pressure rise in Fig.4. As would be expected, the slowest rate of movement of the terminal shock occurs when the blockage ratio is highest (B = 0.211%); however, there is also a difference in shock position for the two tunnels which have almost the same value of B (0.12%). This corresponds more to a constant displacement of the shock position for a given stream Mach number when this is above about 0.99, the rate of shock movement being similar.

Since the correction to the nominal Mach number in the $30\frac{3}{4}$ in. × 14 in. tunnel was larger, and of the opposite sign, compared with the other tunnels some independent check on the validity of the corrected Mach number scale was felt to be necessary. This could be done firstly by comparing the pressures obtained well downstream (p_3 in Fig.5(a)) with those appropriate to the corrected Mach number in all three tunnels. The results are shown in Fig.5(b) and no serious discrepancy exists between data from the $30\frac{3}{4}$ in. × 14 in. and 21 in. × 20 in. tunnels in this Mach number range. Secondly, and at larger values of M_O, the bow-shock position in the $30\frac{3}{4}$ in. × 14 in. tunnel can be compared with the results given in Ref.2 for a model in

the/

---

*In fact, the position of the middle of the pressure rise was used to obtain the flagged symbols contained in Fig.4.

the 17 in. × 14 in. tunnel with $B = 0.204\%$, the terminal shock positions of which are also plotted in Fig.4. Agreement should be expected since the effect of model blockage ratio on bow-wave position is very small[2]. Fig.6 shows that the results from the two tunnels agree well when plotted in terms of the corrected Mach number and it was therefore concluded that the terminal shock displacement at almost constant blockage ratio shown in Fig.4 was a real effect and can presumably be attributed to the different tunnel cross-sections.

In Ref.2, possible reasons for the effect of model blockage ratio on terminal shock position were suggested. For example, it was thought possible that the shock position was controlled directly either by the conditions well downstream, as determined by the pressure ratio p_3/H, or by the conditions just upstream of the shock (p_1/H in Fig.5(a)). As has already been mentioned, p_3/H does in fact recover to almost the correct free-stream value in the Mach number range for which this point could be checked (Fig.5(b)), and this evidence can be supplemented by means of the distribution of pressure along the slotted walls. Fig.5(b) shows that the greatest discrepancy occurs between the 17 in. × 14 in. tunnel results on the one hand and the $30\frac{3}{4}$ in. × 14 in. and 21 in. × 20 in. data on the other. It is true that if the shock position is plotted in terms of a stream Mach number based on p_3/H, then the 17 in. × 14 in. and 21 in. × 20 in. results plotted in Fig.4 would agree more closely for Mach numbers up to about 1.02; the differences between these results and those from the $30\frac{3}{4}$ in. × 14 in. tunnel would not be altered however. It seems likely in fact that the discrepancies in p_3/H between the three tunnels are due to support interference, or inadequate allowance for empty-tunnel pressure gradients or to the difficulty of estimating this ratio from the experimental data. If this were so, it could be concluded that the downstream pressure near the model does not influence the terminal shock position in any simple manner. Tests in the 21 in. × 20 in. tunnel, during which a 2 in. dia boss was placed at about 14 diameters from the model nose supported such a conclusion, since the terminal shock position was unaltered at stream Mach numbers between 0.98 and 1.02.

An alternative suggestion made in Ref.2 was that the change in shock position was largely due to an alteration of shock strength due to the proximity of the tunnel walls. The shock strength close to the model surface is perhaps best considered in terms of the pressure ratios just upstream and downstream of the shock itself (p_1/H, p_2/H) and these quantities can be defined in the manner of Fig.5(a). The actual values are not easy to determine accurately from pressure distributions having a limited number of points. Some improvement results from considering the complete family of curves obtained from one tunnel and estimates of p_1/H and p_2/H are plotted against M_o in Fig.5(c) for all three tunnels. The upstream pressure ratio is similar in the 17 in. × 14 in. and 21 in. × 20 in. tunnels, but for the $30\frac{3}{4}$ × 14 in. working section, p_1/H has a much lower value at stream Mach numbers above about 0.97. The higher local Mach numbers just ahead of the shock in this tunnel are a consequence of the flow expansion along the body which seems to be a marked characteristic of the $30\frac{3}{4}$ in. × 14 in. tunnel results. This can be seen from Fig.1(b), or by comparing pressure distributions at approximately the same stream Mach number, as has been done in Fig.3. The difference in the shape of the pressure distribution upstream of the shock in the different tunnels is well shown on Figs.5(c) and (d), for example, even though the results for the $30\frac{3}{4}$ in. × 14 in. tunnel are affected by the reflection of the front inclined shock from the solid sidewalls (designated $R_{F,S}$). Once again, it appears that the shock position cannot be related simply to the local pressure just upstream.

A surprising feature of Fig.5(c) is the apparent constancy of the ratio p_2/H, for stream Mach numbers greater than about 1.00. The value of about 0.55 shown in Fig.5(c) seems to be independent of both M_o and tunnel. It is true of course that the actual value of p_2/H is

seldom well-defined and that the correct pressure distribution may be somewhat different from that, assumed in drawing the families of curves for the three tunnels. It is felt however that the most likely effect of such a revision would be to alter the value of p_2/H, rather than to alter its constancy with changing tunnel and stream Mach number. However more detailed experiments are required to settle this point. Incidentally the local surface Mach number corresponding to $p_2/H = 0.55$ is about 0.96 which is near the free-stream value at which the rapid rearward movement of the terminal shock commences. This may be entirely coincidental; alternatively it is possible that the terminal shock moves back from a position close to the steep recompression associated with the shoulder only when it can be followed by an expansion back to free-stream pressure conditions. Why this should be the case is not clear.

In view of the relatively low local supersonic Mach number attained ahead of the terminal shock and the turbulent nature of the model boundary layer[2], it might be expected that the full normal shock pressure rise would be obtained at the surface. Schlieren photographs show no separation or undue thickening of the boundary layer as it passes through the shock, though presumably the layer must in part be responsible for the failure to achieve the full pressure rise* (Fig.5(c)). In addition, this effect may in some cases be associated with a local Mach number gradient away from the model surface along the shock front, with an associated reversal of gradient behind the shock. No measurements were made however of the pressure field away from the model surface.

The apparent constancy of the shock downstream pressure, whatever its cause, clearly rules out any possibility of its magnitude determining the terminal-shock position. The same must be true of the rate of pressure fall between the rear of the shock and the attainment of free-stream pressure (i.e., the pressure change from p_2 to p_3). As far as can be judged from the present results, the overall length of this pressure fall measured in terms of model diameters does not greatly increase as the stream Mach number is raised; the pressure difference $p_2 - p_3$ does increase however, and hence the surface gradient steepens, particularly close to the terminal shock. For any given value of M_0, the shape of the pressure-fall curve is similar in all three tunnels (Fig.3(b), for example).

It seems reasonable then to seek for an explanation of variation of terminal-shock position with working-section shape in terms of the flow field between the model nose and the shock itself, and the interaction of this with the closed and partially-open boundaries of the tunnels. The present results, consisting as they do mainly of surface pressure measurements, are not really adequate for this task; moreover the wall pressure-holes are spaced at too wide intervals (about 5 model diameters) to be of value in this connection. Nevertheless, some progress can be made towards explaining the phenomenon.

The effect of the tunnel walls on the pressure distribution between about 2 diameters from the model nose and the terminal shock has already been commented upon briefly. The surface pressures between the shoulder and 2 diameters also show differences between the results from the three tunnels, mainly in the values obtained at $x/d = 0.94$, although such differences tend to be consistent and almost independent of Mach number and hence may well be due to experimental deficiencies.

It/

---

*This failure is most noticeable at the higher values of M_0 in Fig.5(c). Close to, and below, $M_0 = 1.00$, pressure rises greater than the normal shock value are implied, but in this Mach number range the values of p_1/H, and the pressure rise may be influenced by the field from the front inclined shock and the evidence must be considered as inconclusive.

It has been argued that the variation in terminal-shock position for a given stream Mach number may be due to the influence of the tunnel boundaries on the position of the local sonic point on the hemispherical nose. A movement of this towards the stagnation point would result in a larger expansion angle before the shoulder is reached, and a modification of the expansion field reaching the terminal shock, either directly or by reflection from a tunnel wall.

The measured pressure distributions around the nose of the model, when tested in the 17 in. × 14 in. tunnel, are shown in Fig.7(a). Between stream Mach numbers of 0.97 and 1.09, the sonic point moves forward by only about 0.5 degrees, which would have an insignificant effect on the expansion field. This Figure also shows that the supersonic expansion which is attained falls somewhat below the two-dimensional Prandtl-Meyer value.

These results are typical of those from all three tunnels, the sonic point remaining close to $\phi = 59^{\circ}$ in each case. Fig.7(b) shows the pressure distribution around the nose at stream Mach numbers near 1.030; the differences between the three sets of results are small except at the suction peak, which corresponds to $\phi = 90^{\circ}$, $x/d = 0.5$. Similar agreement is obtained at other values of M_o.

The variation in observed pressure for the hole at $x/d = 0.5$ is also shown in Fig.8(a). The rapid fall in pressure near $M_o = 0.90$ is associated with the movement of the suction peak* back to the shoulder (see Fig.7(a)) and the establishment of a well-defined terminal shock. The subsequent fall in pressure at this hole is gradual, but differences exist in the levels recorded in the three tunnels. These may be due to the presence of local disturbances in the tunnel flow at that position, or alternatively the differences could be regarded as indicative of the distortion of the flow field (and in particular the sonic line) around the model due to the tunnel walls.

Similar treatment of the results obtained at other pressure holes (Figs. 8(a) and (b)) show the characteristic trends noted earlier; agreement between the three tunnels when the shock is well upstream of the hole, a similar rate of pressure increase as the shock approaches, the passage of the terminal shock at different stream Mach numbers and a subsequent pressure fall to somewhat dissimilar values in the three tests.

3.2 Pressure-field reflection in the tunnel walls

In free-air conditions the flow-field about the model when the mainstream flow is just subsonic consists of a local supersonic region, bounded on the upstream side by the sonic line and at the downstream end by the terminal shock. The pressure on the model surface is influenced by the expansion around the curved surface of the nose, and also by the 'reflection' of these expansion waves (as compressions) from the sonic line. Thus any distortion of the sonic line due to wall interference will modify the surface pressures, perhaps as sketched in Fig.9(a). This type of interference has been discussed by Pearcey et al[5] for the two-dimensional aerofoil; for the present model it would strictly only be present in quite this form up to the stream Mach number at which the supersonic flow reaches the nearest wall. This occurs at about $M_o = 0.96$ in all three tunnels, despite differences in working-section size. The terminal shock is then about two diameters from the model nose and no serious differences in position exist. It is at stream Mach numbers above this value that the delays in shock movement occur[2]; and hence this type of interference would not seem to be of significance in the present context.

Once/

---

*It is possible that there is a weak shock wave just ahead of the shoulder at slightly lower Mach numbers, but there is not sufficient evidence to distinguish it from the rear of the "low-speed" suction peak.

Once the supersonic flow region reaches a wall, some of the expansion waves reflect from this instead of the sonic line. From a solid sidewall, expansion waves would result, whilst the reflection from a slotted wall would consist of a mixture of expansion and compression waves the relative intensity of which depends on the slot configuration. It is sufficiently accurate to consider the supersonic region as extending to both solid and slotted walls at about the same stream Mach number in the present tests, and thus the magnitude of the interference effect depends on the distance away, and composition of, the surrounding tunnel walls.

The proximity of a tunnel wall may influence the shape of the sonic line itself, and because of this, the position at which expansion waves are reflected back on to the model surface (Fig.9(b)). If the sonic line moves upstream, to form a shape more consistent with the parabola-like line obtained with a single-sided convergent-divergent nozzle, the reflected waves will reach the model further downstream, thus reducing the pressure at a given point, compared with the free-air case. At some stage the sonic line moves sufficiently far forward for the reflection from the wall to influence the model surface upstream of the shock directly. Subsequently the influence of the reflections from the sonic line diminishes compared with those from the walls, until at supersonic stream speeds the sonic line is inclined forward and now terminates the local subsonic region behind the bow wave. In Fig.9(c), the sonic line is shown as still reaching the wall so that bow-wave reflection cannot occur, although the wall between the bow-wave and the sonic line may influence the model.

The primary source of interference however would seem to be the reflections from the tunnel wall. If the wall is solid and close, the local pressures ahead of the shock should fall; the presence of a nearby slotted wall would diminish this effect somewhat.

This simple flow model is nevertheless consistent with the experimental results. In the 17 in. × 14 in. and 21 in. × 20 in. tunnels, the reflected waves from the solid sidewalls are probably counterbalanced to some extent by those from the slotted liners, since the open area ratio is fairly large, and the pressure ahead of the terminal shock remains almost constant or falls only slowly. In the $30\frac{3}{4}$ in. × 14 in. tunnel, the slotted walls being further away can have less effect and the flow field is dominated by the expansion field reflected from the solid walls. As a result, the surface pressures ahead of the shock are lower, (see Fig.3(c), for example).

To pursue this point further, the tests in the 21 in. × 20 in. tunnel were extended to measure the pressures on the model when it was moved progressively towards either a solid or a slotted wall. The results obtained are listed in Table 2(d) whilst those for M_o = 1.022 are plotted in Figs.10(a) and (b). The displacement of the model is accompanied unfortunately by a forward movement of the intersection of the reflection of the front-inclined shock with the model, (R_F), complicating the shape of pressure distributions. However between 2.5 and 5 diameters from the nose of the model there is a region which may be regarded as being sensitive to wall-reflection effects. Thus as the slotted wall is approached (Fig.10(a)) the local pressure in this region falls only slightly; on the other hand by approaching the solid wall (Fig.10(b)), the pressures can be made to fall rapidly. In these tests, of course, the increased effect due to approaching one wall is counterbalanced to some extent by a reduced effect from the opposite wall, and it is thus not possible to use the results shown in Fig.10 to make quantitative deductions about changes in tunnel size and shape. The general conclusions about wall proximity would seem to be substantiated however.

Two further points emerge from these off-centre tests. Firstly the intersection of the reflected front-inclined shock occurs at $x/d = 5$, when the model is 6 inches from a slotted wall, but at about $x/d = 7$ when it is the same distance from a solid wall. This is perhaps additional evidence of higher local Mach numbers between the model and the wall in the latter case, a state of affairs consistent with the different reflection characteristics of the two types of wall.

The second concerns the position of the terminal shock for the tests presented in Fig.10. This corresponds to the final pressure rise in the surface distributions, just before the fall back to free-stream pressure. When the model is at the tunnel centre, the shock is at approximately $x/d = 7.5$. A pressure rise still occurs at this position when the model is displaced 4.5 in. towards the slotted wall ($b = 6$ in. in Fig.10(a)), and there is a corresponding shock on the schlieren photograph. The interference due to the reflection of the front-inclined wave modifies both the pressures upstream and downstream of the shock. As the solid wall is approached (Fig.10(b)) a small pressure rise still seems to occur near $x/d = 7.5$ and this seems to correspond to the presence of a terminal shock visible on the schlieren photographs. The local Mach number near the model however is just subsonic as a result of the effect of the reflected front shock. The latter incidentally is far stronger in Fig.10(b). It thus seems that the terminal shock position in the tunnel is not greatly altered by offsetting the present model, though some forward movement was noted for very small blockage ratios in Ref.2.

3.3 Some factors influencing terminal-shock position

Although the foregoing remarks provide some explanation of the shape of the observed pressure distributions upstream of the terminal shock, they do not provide a direct explanation of why the shock position should be different in the three tunnels.

Consider first the flow about a hemisphere-cylinder in inviscid unbounded flow at speeds approaching sonic speed. The surface distribution of pressure is probably similar to that sketched in Fig.11(a), the terminal shock* moving rearward rapidly and diminishing in strength until at $M_0 = 1.0$ it disappears. The shock position cannot depend on any downstream condition since there is no obvious characteristic length**. Nevertheless the height of the sonic boundary must be fixed for any given stream Mach number (dependent only on the body diameter) and it seems reasonable to relate the shock position to this, the shock moving rearward as the supersonic region expands away from the body.

This argument may be extended to suggest that the terminal shock itself results from the coalescence of the compression wave system originating from the sonic line, and that the shock would then become weaker as the stream Mach number approaches unity and the sonic line straightens.

In the constrained flow of the transonic tunnel the rearward movement of the terminal shock is delayed so that it persists at supersonic stream speeds. The comparison between free-air pressure distributions at Mach numbers just above one and those likely to be obtained in the tunnel are sketched in Fig.11(b).

It/

---

*The terminal shock in this Figure is assumed to have the full normal-shock pressure rise, followed by a slow pressure fall to free-stream pressure.

**In viscous flow it may be argued that the rate of boundary-layer growth provides some characteristic length. This would seem to imply fundamental changes in shock position due to the presence of a boundary layer. An explanation in terms of the height of the supersonic region seems more reasonable.

It seems difficult to attribute the same mechanism for the formation of the shock in the tunnel at low supersonic speeds as in free-air at subsonic speeds. The flow-field differences which produce the pressure-distribution changes of Fig.11(b) are the reflection of expansion waves from the tunnel wall (discussed earlier) and the pressure conditions imposed by the plenum chamber at the slotted wall. The latter may be regarded crudely as attempting to impose the free-stream pressure everywhere along the wall and thus to minimise the perturbations produced by the model. If the shock is strong at the wall (i.e., the latter is close to the model) and the rate of pressure fall to free-stream conditions is fixed, say, only by the value of M_o, then a forward shock position would allow free-stream pressure to be obtained in the shortest downstream distance. If the slotted wall is far from the model, the shock will be rather weaker, the pressure change completed in a smaller distance, and the shock need not be so far forward. Fig.12 illustrates these points.

This hypothesis is difficult to apply to a tunnel which has both slotted and solid walls, but in its simplest form one would expect the shock position to be determined by the average distance of the slotted walls from the model and the surface Mach number upstream of the terminal shock to be influenced by the nearness of the solid walls. Thus an approximate shock-position parameter is x_s/h, where x_s is the distance from the model nose and h is the half-height of the tunnel*. Alternatively, the shock movement from the condition when the supersonic flow first reaches the wall may be more relevant; this corresponds to a parameter G which for the present tests is defined as

$$G = \frac{d}{h}\left[\frac{x_s}{d} - 2\right].$$

The shock positions for the model in the three different tunnels have been plotted in this form in Fig.13. The agreement between the results from the tunnels of 14 in. width is very good, the slope of the curves being similar. The 21 in. × 20 in. results agree well up to stream Mach numbers of about 1.02, but thereafter the rate of shock movement is too large to give agreement. This may be due to the influence of the greater tunnel width in this case. Fig.14 shows a corresponding replot of the results presented in Fig.5 of Ref.2, where similar models were tested in the 17 in. × 14 in. tunnel at blockage ratios varying between 0.204% and 0.0021%. For these results the numerical constant in the equation for G has been modified to allow for the different positions of the terminal shock along the model when the supersonic flow first reaches the wall, $(x_s/d)_o$. The results collapse in a satisfactory manner once the shock has moved an appreciable distance from the position $(x_s/d)_o$ so that errors in estimating the change in shock position are no longer dominant.

4. Nose Drag

The pressure distributions on the hemispherical nose were integrated to give the total axial force, F, and these results, as the non-dimensional force coefficient, C_F, are shown in Fig.15. C_F is defined by

$$C_F = \frac{F}{H.\frac{1}{4}\pi d^2}.$$

At/

---

*Prior recognition of the significance of the parameter x_s/h must be accorded to Mr. E. P. Sutton of Cambridge University who has analysed results from tests on ogive-cylinder models in a tunnel slotted on all four walls.

At Mach numbers between 0.7 and 0.9 C_F falls approximately linearly. Then there is a small but rapid decrease after which the curve quickly flattens out to a value of about 0.67. No results are available at Mach numbers higher than 1.10 except for that at 2.45^4. At this Mach number $C_F = 0.164$.

The sudden decrease in C_F at $M \simeq 0.90$ is due to the change in the shape of the pressure distribution just ahead of the shoulder. It is shown in Fig.7(a) that the peak suction moves back rapidly to the shoulder at a Mach number of about 0.90 producing a sudden reduction in the pressure on the area near the shoulder. This is responsible for the sudden reduction in C_F. It is also shown in this Figure that there is very little change in the pressure distribution with further increase of Mach numbers up to 1.089.

From the comparison of pressure distributions at $M_o = 1.03$ (Fig.7(b)) it is clear that at this Mach number there are no significant differences between the results from the three tunnels. At certain other Mach numbers (e.g., at $M_o = 0.80$) the agreement is not quite as good although the discrepancies are always less than 0.003 in C_F, which is about the limit of accuracy of the results. Within this limit there is a very slight trend for the axial force to be higher in the $30\frac{3}{4}$ in. $\times$ 14 in. and lower in the 21 in. $\times$ 20 in. than it is in the 17 in. $\times$ 14 in. tunnel.

For comparison with other results the axial force curve is replotted as a conventional drag coefficient, C_D, where

$$C_D = C_F \cdot \frac{H}{\frac{1}{2}\rho U^2} - \frac{p_s}{\frac{1}{2}\rho U^2} .$$

The variation of C_D with Mach number is shown in Fig.16 and the values are given in Table 3. Also shown in this Figure are the free-flight drag coefficients on a hemispherical-nosed body obtained by Wallskog and Hart[7]. A direct comparison is not possible because their body had a parabolic afterbody. However, this afterbody had a very small boattail, the base area, after five diameters, being 0.19 of the maximum diameter so that a comparison of general trends is justified.

The variation of C_D over the entire Mach number range up to 3.0 is shown in the inset to Fig.16. This is based on the present results and those of Refs. 4 and 8. In addition the value at very low speeds, about 0.005, can be obtained from Ref.9.

5. Concluding Remarks

In the preceding pages some simple tests made in three N.P.L. slotted-wall tunnels on a hemisphere-cylinder model have been analysed. It has been shown that the delay in the rearward movement of the terminal shock with increasing stream Mach number does not depend simply on the blockage ratio, but rather on the distance of the nearest slotted wall in model diameters. Though the distance away of the solid wall complicates the problem, its chief contribution seems to be to influence the local Mach numbers on the model upstream of the terminal shock. It seems that neither the shock strength, nor the pressure far downstream from the shock directly govern the shock position. The position of the sonic point on the nose of the model is almost unchanged by alteration in stream Mach number or tunnel size.

The arguments used in the present text must be considered as tentative until substantiated by more detailed experimental data. If they, and the conclusions drawn, are substantially correct, it should be possible to generalise beyond the present type of model and working section configuration.

It/

It was stated in Section 2.3 that no theoretical corrections have been applied to allow for the effects of wall constraint. The present results could be subject to some form of tunnel interference analogous to the type discussed by Berndt[6] for slender bodies in circular slotted tunnels. He suggests that sonic flow about the model should occur when the Mach number upstream is $1 - \Delta M_o$, where ΔM_o is a correction dependant upon the slot configuration, model length and fineness ratio. It is not possible to calculate accurately the appropriate correction for the present model and tunnels; moreover it is obvious that sonic flow conditions are never really attained during the tests on a hemisphere cylinder. A Mach number correction of the type proposed by Berndt however would modify the values of M_o used in the present report and hence the main arguments put forward. It is felt that the agreement between the downstream pressures on the body (Fig.5(b)) and the bow-wave position (Fig.6) is such that any additional Mach number correction must be very small (say less than 0.003). This is considerably lower than the corrections which result from making certain simplifying assumptions in Berndt's analysis; at $M = 1$, these are between 0.02 and 0.03 for the three tunnels.

6.   Acknowledgements

References/

References

No.	Author(s)	Title, etc.
1	F. E. Roe	Some aspects of transonic tunnel operation in industry. Journ. Royal Ae. Soc. Vol. 62, p.16. 1958.
2	E. W. E. Rogers and I. M. Hall	Some experiments with static tubes at transonic speeds in a slotted-wall wind tunnel. A.R.C. C.P.430. July, 1958.
3	W. A. Page	Experimental study of the equivalence of transonic flow about slender cone-cylinders of circular and elliptic cross-section. N.A.C.A. TN.4233. 1958.
4	I. M. Hall, E. W. E. Rogers and Miss B. M. Davis	Experiments with inclined blunt-nosed bodies at M_O = 2.45. A.R.C. R. & M.3128. August, 1957.
5	H. H. Pearcey, C. S. Sinnott and J. Osborne	Some effects of wind-tunnel interference observed in tests on two-dimensional aerofoils at high subsonic and transonic speeds. NPL/Aero/373. 1959.
6	S. B. Berndt	Theoretical aspects of the calibration of transonic test sections. Z.A.M.P. Vol.IXb Fasc 5/6, p.105. 1958.
7	W. A. Wallskog and R. G. Hart	Investigation of the drag of blunt-nosed bodies of revolution in free flight at Mach numbers from 0.6 to 2.3. N.A.C.A. RM L53D14a. NACA/TIL/3760. 1953.
8	L. T. Chauvin	Pressure distribution and pressure drag for a hemispherical nose at Mach numbers 2.05, 2.54, and 3.04. N.A.C.A. RM L52K06. NACA/TIB/3547. 31st December, 1952 A.R.C.16,043. 10th July, 1953.
9	H. Rouse, J. S. McNown and E. Hsu	Cavitation tests on a systematic series of torpedo heads. Iowa Institute of Hydraulic Research, Iowa University. 1945.

—

Table 1

Position of Pressure Holes on Model

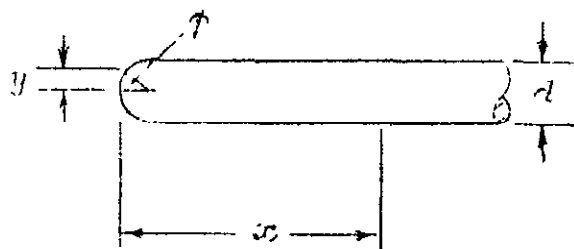| Hole No.	x/d	y/d	ϕ
1	0	0	0
2	0.02	0.13	15°
3	0.07	0.25	30°
4	0.15	0.35	45°
5	0.25	0.43	60°
6	0.37	0.48	75°
7	0.50	0.50	90°
8	0.94		
9	1.88		
10	2.81		
11	3.75		
12	4.69		
13	5.63		
14	6.56		
15	7.50		
16	8.44		
17	9.38		
18	10.31		
19	11.25		
20	12.19		
21	13.13		
22	14.06		

Table 2(a)

Distribution of Pressure on Hemisphere-Cylinder Model in 17 in. × 14 in. Working Section

p = measured static pressure   H = stream total pressure

M_O	x/d =	0	0.02	0.07	0.15	0.25	0.37	0.50	0.94	1.88	2.81	3.75
0.700	p/H =	1.000	0.972	0.873	0.756	0.597	0.509	0.549	0.697	0.713	0.716	0.717
0.750		1.000	0.970	0.864	0.737	0.566	0.475	0.514	0.620	0.683	0.684	0.685
0.801		1.000	0.968	0.855	0.722	0.541	0.451	0.474	0.533	0.655	0.652	0.653
0.821		1.000	0.967	0.852	0.716	0.533	0.437	0.458	0.502	0.645	0.640	0.640
0.842		1.000	0.967	0.850	0.712	0.529	0.422	0.443	0.475	0.636	0.629	0.628
0.852		1.000	0.966	0.848	0.708	0.520	0.399	0.428	0.451	0.625	0.618	0.615
0.882		1.000	0.965	0.846	0.704	0.515	0.372	0.407	0.428	0.609	0.607	0.603
0.892		1.000	0.965	0.844	0.703	0.513	0.362	0.397	0.417	0.601	0.601	0.597
0.903		1.000	0.966	0.844	0.701	0.511	0.351	0.258	0.337	0.599	0.589	0.589
0.923		1.000	0.964	0.842	0.698	0.507	0.347	0.251	0.317	0.600	0.580	0.577
0.944		1.000	0.965	0.842	0.697	0.505	0.344	0.245	0.311	0.593	0.577	0.568
0.954		1.000	0.964	0.841	0.696	0.503	0.342	0.243	0.309	0.577	0.577	0.565
0.964		1.000	0.964	0.841	0.695	0.502	0.342	0.240	0.308	0.524	0.574	0.564
0.974		1.000	0.964	0.840	0.694	0.501	0.340	0.237	0.308	0.476	0.563	0.563
0.984		1.000	0.965	0.841	0.695	0.502	0.341	0.235	0.307	0.470	0.536	0.557
0.994		1.000	0.964	0.840	0.693	0.500	0.339	0.232	0.306	0.466	0.501	0.546
1.005		1.000	0.965	0.840	0.694	0.500	0.339	0.229	0.305	0.462	0.495	0.501
1.016		1.000	0.965	0.840	0.694	0.500	0.339	0.228	0.304	0.459	0.491	0.495
1.028		1.000	0.965	0.840	0.693	0.499	0.338	0.225	0.303	0.456	0.485	0.489
1.039		1.000	0.963	0.839	0.692	0.498	0.337	0.223	0.302	0.453	0.481	0.484
1.050		1.000	0.964	0.839	0.692	0.498	0.337	0.224	0.303	0.452	0.479	0.482
1.060		1.000	0.965	0.840	0.693	0.500	0.339	0.229	0.303	0.454	0.479	0.482
1.070		1.000	0.963	0.839	0.693	0.499	0.337	0.224	0.304	0.457	0.479	0.472
1.089		1.000	0.964	0.839	0.691	0.497	0.335	0.218	0.300	0.452	0.491	0.488
1.109		1.000	0.962	0.835	0.687	0.515	0.332	0.207	0.293	0.427	0.473	0.485

Table 2(a) (contd.)

M_O	x/d =	4.69	5.63	6.56	7.50	8.44	9.38	10.31	11.25	12.19	13.13	14.06
0.700	p/H =	0.718	0.720	0.721	0.721	0.721	0.721	0.721	0.720	0.720	0.721	0.722
0.750		0.686	0.688	0.690	0.689	0.689	0.689	0.689	0.688	0.688	0.689	0.691
0.801		0.653	0.656	0.658	0.657	0.657	0.658	0.657	0.656	0.656	0.657	0.659
0.821		0.640	0.642	0.644	0.643	0.643	0.644	0.643	0.642	0.642	0.643	0.645
0.842		0.627	0.629	0.631	0.630	0.630	0.631	0.630	0.629	0.629	0.630	0.633
0.852		0.615	0.616	0.618	0.617	0.617	0.618	0.617	0.616	0.617	0.618	0.620
0.882		0.602	0.603	0.605	0.604	0.604	0.605	0.604	0.603	0.603	0.605	0.607
0.892		0.596	0.597	0.599	0.598	0.599	0.600	0.598	0.597	0.597	0.598	0.601
0.903		0.588	0.590	0.592	0.591	0.591	0.592	0.591	0.590	0.591	0.592	0.595
0.923		0.576	0.578	0.580	0.579	0.579	0.580	0.579	0.578	0.578	0.579	0.583
0.944		0.564	0.565	0.567	0.565	0.566	0.567	0.566	0.565	0.565	0.567	0.569
0.954		0.559	0.560	0.561	0.559	0.560	0.561	0.560	0.559	0.559	0.561	0.564
0.964		0.556	0.555	0.555	0.553	0.553	0.554	0.554	0.552	0.553	0.554	0.558
0.974		0.554	0.550	0.550	0.547	0.547	0.548	0.547	0.546	0.547	0.548	0.552
0.984		0.553	0.548	0.546	0.542	0.541	0.542	0.541	0.540	0.540	0.542	0.545
0.994		0.550	0.547	0.543	0.537	0.536	0.537	0.536	0.535	0.535	0.536	0.541
1.005		0.546	0.548	0.542	0.534	0.531	0.531	0.530	0.528	0.529	0.531	0.536
1.016		0.496	0.549	0.545	0.534	0.527	0.525	0.524	0.523	0.522	0.525	0.533
1.028		0.488	0.488	0.552	0.541	0.529	0.521	0.515	0.512	0.514	0.521	0.530
1.039		0.483	0.482	0.485	0.550	0.537	0.522	0.513	0.504	0.503	0.507	0.521
1.050		0.480	0.478	0.476	0.481	0.553	0.535	0.518	0.503	0.494	0.499	0.505
1.060		0.477	0.473	0.472	0.463	0.500	–	0.533	0.516	0.501	0.490	0.492
1.070		0.473	0.471	0.467	0.458	0.452	0.517	0.539	0.528	0.519	0.508	0.499
1.089		0.473	0.459	0.453	0.450	0.445	–	0.473	0.516	0.497	0.479	0.511
1.109		0.492	0.474	0.456	0.437	0.430	–	0.452	0.472	0.497	0.485	0.464

Table 2(b)

Distribution of Pressure on Hemisphere–Cylinder Model in $30\frac{3}{4}$ in. × 14 in. Working Section

p = measured static pressure   H = stream total pressure

M_o	x/d =	0	0.02	0.07	0.15	0.25	0.37	0.50	0.94	1.88	2.81	3.75
0.798	p/H =	1.000	0.971	0.860	0.724	0.541	0.467	0.483	0.548	0.661	0.659	0.661
0.897		1.000	0.970	0.850	0.701	0.508	0.360	0.391	0.414	0.596	0.601	0.595
0.946		1.000	0.969	0.846	0.696	0.499	0.340	0.243	0.328	0.581	0.579	0.568
0.965		1.000	0.969	0.846	0.693	0.496	0.337	0.244	0.311	0.478	0.563	0.565
0.975		1.000	0.968	0.845	0.694	0.497	0.336	0.242	0.307	0.471	0.517	0.555
0.984		1.000	0.968	0.844	0.691	0.494	0.335	0.240	0.313	0.465	0.500	0.527
0.989		1.000	0.967	0.844	0.694	0.497	0.335	0.239	0.308	0.465	0.496	0.500
0.993		1.000	0.970	0.846	0.694	0.497	0.341	0.240	0.307	0.466	0.495	0.498
0.998		1.000	0.969	0.845	0.693	0.496	0.336	0.240	0.307	0.467	0.492	0.496
1.003		1.000	0.968	0.844	0.692	0.495	0.338	0.241	0.304	0.461	0.491	0.493
1.008		1.000	0.968	0.845	0.692	0.495	0.334	0.238	0.307	0.460	0.489	0.491
1.012		1.000	0.969	0.849	0.693	0.496	0.340	0.240	0.308	0.459	0.488	0.490
1.017		1.000	0.968	0.845	0.693	0.496	0.334	0.237	0.307	0.458	0.487	0.488
1.021		1.000	0.968	0.846	0.692	0.498	0.337	0.240	0.308	0.458	0.487	0.487
1.031		1.000	0.969	0.845	0.693	0.496	0.337	0.237	0.308	0.457	0.484	0.484
1.049		1.000	0.968	0.844	0.692	0.495	0.334	0.236	0.308	0.455	0.483	0.483
1.068		1.000	0.968	0.844	0.692	0.495	–	0.235	0.309	0.458	0.482	0.479
1.088		1.000	0.968	0.843	0.691	0.494	0.335	0.233	0.306	0.454	0.482	0.479

Table 2(b) (contd.)

M_o	x/d =	4.69	5.63	6.56	7.50	8.44	9.38	10.31	11.25	12.19	13.13	14.06
0.798	p/H =	0.665	0.662	0.665	0.664	0.665	0.666	0.666	0.666	0.666	0.668	0.671
0.897		0.595	0.595	0.598	0.596	0.598	0.599	0.599	0.600	0.601	0.602	0.606
0.946		0.565	0.562	0.565	0.563	0.565	0.569	0.566	0.566	0.567	0.568	0.571
0.965		0.557	0.552	0.552	0.551	0.551	0.552	0.552	0.551	0.552	0.554	0.557
0.975		0.554	0.549	0.546	0.543	0.543	0.544	0.542	0.541	0.541	0.543	0.544
0.984		0.551	0.548	0.545	0.540	0.539	0.539	0.538	0.537	0.538	0.539	0.542
0.989		0.542	0.548	0.545	0.538	0.536	0.536	0.534	0.532	0.532	0.533	0.535
0.993		0.495	0.548	0.548	0.541	0.537	0.534	0.532	0.529	0.528	0.530	0.531
0.998		0.492	0.499	0.551	0.542	0.537	0.533	0.530	0.527	0.526	0.527	0.529
1.003		0.490	0.485	0.537	0.548	0.540	0.534	0.528	0.524	0.523	0.526	0.525
1.008		0.487	0.485	0.485	0.549	0.542	0.534	0.528	0.521	0.518	0.521	0.524
1.012		0.486	0.480	0.479	0.533	0.548	0.539	0.531	0.522	0.517	0.515	0.517
1.017		0.484	0.479	0.473	0.471	9.541	0.545	0.535	0.524	0.518	0.513	0.511
1.021		0.484	0.482	0.475	0.463	0.502	0.546	0.542	0.530	0.521	0.515	0.510
1.031		0.480	0.477	0.471	0.461	0.492	0.490	0.545	0.549	0.534	0.523	0.515
1.049		0.478	0.473	0.468	0.452	0.450	0.479	0.477	0.475	0.471	0.480	0.542
1.068		0.478	0.477	0.472	0.454	0.454	0.465	0.460	0.462	0.462	0.461	0.465
1.088		0.473	0.468	0.465	0.452	0.451	0.483	0.473	0.455	0.446	0.447	0.451

Table 2(c)

Distribution of Pressure on Hemisphere-Cylinder Model in 21 in. × 20 in. Working Section

p = measured static pressure   H = stream total pressure

M_0	x/d =	0	0.02	0.07	0.15	0.25	0.37	0.50	0.94	1.88	2.81	3.75
0.803	p/H =	1.000	0.966	0.853	0.714	0.534	0.450	0.465	0.530	0.650	0.648	0.648
0.903		1.000	0.968	0.846	0.699	0.508	0.350	0.258	0.341	0.598	0.590	0.589
0.953		1.000	0.967	0.843	0.693	0.501	0.342	0.235	0.320	0.574	0.578	0.566
0.963		1.000	0.967	0.843	0.693	0.500	0.342	0.232	0.318	0.508	0.573	0.565
0.973		1.000	0.967	0.842	0.692	0.499	0.340	0.230	0.316	0.476	0.562	0.564
0.983		1.000	0.967	0.842	0.692	0.498	0.340	0.230	0.316	0.471	0.529	0.555
0.988		1.000	0.967	0.842	0.691	0.498	0.339	0.229	0.314	0.468	0.508	0.544
0.993		1.000	0.967	0.842	0.691	0.498	0.339	0.228	0.313	0.467	0.505	0.536
0.998		1.000	0.967	0.842	0.692	0.500	0.343	0.226	0.314	0.464	0.501	0.509
1.003		1.000	0.967	0.842	0.691	0.497	0.339	0.227	0.313	0.464	0.500	0.507
1.008		1.000	0.967	0.841	0.691	0.497	0.338	0.224	0.313	0.461	0.496	0.504
1.013		1.000	0.967	0.842	0.690	0.496	0.337	0.224	0.312	0.460	0.494	0.501
1.017		1.000	0.967	0.841	0.691	0.496	0.337	0.223	0.312	0.459	0.493	0.499
1.022		1.000	0.967	0.842	0.691	0.498	0.339	0.226	0.313	0.459	0.492	0.499
1.027		1.000	0.967	0.841	0.690	0.497	0.339	0.224	0.312	0.458	0.490	0.495
1.032		1.000	0.967	0.841	0.690	0.497	0.339	0.225	0.313	0.458	0.490	0.495
1.037		1.000	0.967	0.841	0.690	0.496	0.337	0.224	0.311	0.456	0.488	0.491
1.042		1.000	0.967	0.841	0.690	0.497	0.339	0.224	0.312	0.457	0.487	0.492
1.060		1.000	0.967	0.840	0.690	0.496	0.338	0.222	0.312	0.460	0.496	0.497
1.078		1.000	0.967	0.839	0.686	0.492	0.333	0.213	0.303	0.440	0.476	0.493

Table 2(c) (contd.)

M_O	x/d =	4.69	5.63	6.56	7.50	8.44	9.38	10.31	11.25	12.19	13.13	14.06
0.803	p/H =	0.648	0.649	0.650	0.650	0.650	0.651	0.651	0.649	0.649	0.649	0.650
0.903		0.589	0.590	0.591	0.590	0.590	0.591	0.591	0.589	0.589	0.590	0.591
0.953		0.561	0.559	0.560	0.559	0.559	0.559	0.559	0.557	0.557	0.557	0.558
0.963		0.557	0.555	0.554	0.552	0.552	0.553	0.552	0.550	0.550	0.550	0.550
0.973		0.556	0.552	0.550	0.547	0.547	0.547	0.547	0.545	0.545	0.545	0.545
0.983		0.555	0.550	0.547	0.543	0.542	0.542	0.541	0.539	0.539	0.538	0.539
0.988		0.550	0.549	0.545	0.540	0.538	0.537	0.536	0.534	0.534	0.534	0.534
0.993		0.548	0.548	0.544	0.539	0.537	0.536	0.535	0.532	0.532	0.532	0.532
0.998		0.530	0.546	0.545	0.539	0.535	0.532	0.531	0.528	0.528	0.527	0.527
1.003		0.515	0.544	0.544	0.539	0.534	0.531	0.529	0.526	0.526	0.526	0.526
1.008		0.505	0.526	0.546	0.540	0.535	0.529	0.526	0.522	0.522	0.523	0.523
1.013		0.502	0.504	0.543	0.542	0.536	0.529	0.523	0.519	0.518	0.519	0.520
1.017		0.500	0.500	0.508	0.545	0.539	0.531	0.524	0.517	0.515	0.514	0.515
1.022		0.498	0.498	0.499	0.510	0.547	0.539	0.528	0.519	0.513	0.511	0.511
1.027		0.495	0.495	0.495	0.492	0.540	0.544	0.532	0.520	0.514	0.509	0.508
1.032		0.494	0.494	0.494	0.491	0.509	0.547	0.536	0.523	0.515	0.509	0.506
1.037		0.491	0.491	0.490	0.486	0.485	0.512	0.547	0.534	0.523	0.514	0.506
1.042		0.490	0.487	0.489	0.485	0.483	0.482	0.542	0.542	0.530	0.520	0.511
1.060		0.488	0.480	0.475	0.474	0.474	0.471	0.467	0.462	0.521	0.523	0.509
1.078		0.507	0.494	0.483	0.470	0.460	0.454	0.456	0.451	0.451	0.503	0.509

Table 2(d)

Distribution of Pressure on Hemisphere-Cylinder Model in 21 in. × 20 in. Working Section when Moved from the Tunnel Centre-Line

(i) Movement towards solid wall at constant stream Mach number

Distance of model from solid wall	M_o	x/d	0	0.02	0.07	0.15	0.25	0.37	0.50	0.94	1.88	2.81	3.75
a = 4"	1.022		1.000	0.966	0.841	0.590	0.497	0.337	0.223	0.311	0.453	0.482	0.478
5"	1.022		1.000	0.966	0.839	0.695	0.503	0.338	0.229	0.306	0.456	0.487	0.487
7"	1.022		1.000	0.964	0.835	0.688	0.501	0.345	0.223	0.313	0.456	0.491	0.495
10.5" (C.L.)	1.022		1.000	0.967	0.842	0.691	0.498	0.339	0.226	0.313	0.459	0.492	0.499

Table 2(d) (contd.)

Distance of model from solid wall	M_o	x/d	4.69	5.63	6.56	7.50	8.44	9.38	10.31	11.25	12.19	13.13	14.06
a = 4"	1.022		0.469	0.513	0.532	0.533	0.531	0.529	0.525	0.519	0.516	0.512	0.511
5"	1.022		0.481	0.477	0.529	0.537	0.534	0.531	0.526	0.520	0.516	0.512	0.512
7"	1.022		0.494	0.492	0.493	0.541	0.540	0.534	0.526	0.518	0.514	0.511	0.511
10.5" (C.L.)	1.022		0.498	0.498	0.499	0.510	0.547	0.539	0.528	0.519	0.513	0.511	0.511

<u>Table 2(d)</u>

(ii) Effect of changes in stream Mach number of constant model position

Distance of model from solid wall	x/d M_o	0	0.02	0.07	0.15	0.25	0.37	0.50	0.94	1.88	2.81	3.75
a = 7"	1.003	1.000	0.964	0.835	0.689	0.502	0.346	0.227	0.314	0.461	0.499	0.505
7"	1.022	1.000	0.964	0.835	0.688	0.501	0.345	0.223	0.313	0.456	0.491	0.495
7"	1.032	1.000	0.964	0.835	0.689	0.501	0.345	0.222	0.312	0.454	0.488	0.491
7"	1.042	1.000	0.964	0.835	0.689	0.501	0.345	0.220	0.311	0.454	0.485	0.487

<u>Table 2(d)</u> (contd.)

Distance of model from solid wall	x/d M_o	4.69	5.63	6.56	7.50	8.44	9.38	10.31	11.25	12.19	13.13	14.06
a = 7"	1.003	0.518	0.547	0.544	0.539	0.534	0.532	0.529	0.527	0.526	0.526	0.526
7"	1.022	0.494	0.492	0.493	0.541	0.540	0.534	0.526	0.518	0.514	0.511	0.511
7"	1.032	0.490	0.487	0.486	0.484	0.536	0.539	0.533	0.523	0.515	0.509	0.505
7"	1.042	0.486	0.484	0.481	0.476	0.477	0.528	0.530	0.526	0.525	0.520	0.510

<u>Table 2(d) (iii)</u>/

Table 2(d)

(iii)   Movement towards slotted wall at constant stream Mach number

Distance of model from slotted wall	M_0	x/d 0	0.02	0.07	0.15	0.25	0.37	0.50	0.94	1.88	2.81	3.75
b = 6"	1.022	1.000	0.967	0.843	0.690	0.494	0.336	0.227	0.307	0.458	0.489	0.496
7"	1.022	1.000	0.967	0.843	0.691	0.494	0.334	0.236	0.299	0.459	0.489	0.496
10" (C.L.)	1.022	1.000	0.967	0.842	0.691	0.498	0.339	0.226	0.313	0.459	0.492	0.499

Table 2(d) (iii) (contd.)

Distance of model from slotted wall	M_0	x/d 4.69	5.63	6.56	7.50	8.44	9.38	10.31	11.25	12.19	13.13	14.06
b = 6"	1.022	0.500	0.518	0.513	0.521	0.531	0.526	0.522	0.517	0.515	0.512	0.509
7"	1.022	0.497	0.502	0.515	0.523	0.533	0.528	0.523	0.516	0.514	0.511	0.509
10" (C.L.)	1.022	0.498	0.498	0.499	0.510	0.547	0.539	0.528	0.519	0.513	0.511	0.511

Table 2(d)

(iv)   Effect of changes in stream Mach number at constant model position

Distance of model from slotted wall	M_O \ x/d	0	0.02	0.07	0.15	0.25	0.37	0.50	0.94	1.88	2.81	3.75
b = 7"	1.003	1.000	0.967	0.844	0.691	0.461	0.334	0.237	0.300	0.463	0.498	0.507
7"	1.022	1.000	0.967	0.843	0.691	0.494	0.334	0.236	0.299	0.459	0.489	0.496
7"	1.032	1.000	C.967	0.843	0.691	0.494	0.334	0.233	0.300	0.456	0.486	0.492
7"	1.042	1.000	0.967	0.844	0.692	0.495	0.334	0.231	0.301	0.456	0.485	0.488

Table 2(d) (iv) (contd.)

Distance of model from slotted wall	M_O \ x/d	4.69	5.63	6.56	7.50	8.44	9.38	10.31	11.25	12.19	13.13	14.06
b = 7"	1.003	0.536	0.541	0.539	0.535	0.532	0.529	0.528	0.525	0.525	0.525	0.525
7"	1.022	0.497	0.502	0.515	0.523	0.533	0.528	0.523	0.516	0.514	0.511	0.509
7"	1.032	0.494	0.495	0.512	0.502	0.503	0.534	0.530	0.521	0.513	0.507	0.505
7"	1.042	0.487	0.489	0.496	0.500	0.492	0.488	0.515	0.528	0.529	0.521	0.511

Table 3

Nose Drag Coefficients

17 in. × 14 in. working section		$30\frac{3}{4}$ in. × 14 in. working section		21 in. × 20 in. working section	
M_o	C_D	M_o	C_D	M_o	C_D
0.700	0.105				
0.750	0.144				
0.801	0.192	0.798	0.201	0.803	0.180
0.821	0.209				
0.842	0.232				
0.862	0.245				
0.882	0.258				
0.892	0.266				
		0.897	0.274		
0.903	0.263			0.903	0.261
0.923	0.286				
0.944	0.315	0.946	0.315		
0.954	0.325			0.953	0.322
0.964	0.338	0.965	0.338	0.963	0.334
0.974	0.350	0.975	0.350	0.973	0.347
0.984	0.366	0.984	0.359	0.983	0.360
0.994	0.375	0.993	0.378	0.993	0.373
1.005	0.391	1.003	0.387	1.003	0.386
1.016	0.405	1.012	0.402	1.013	0.397
1.028	0.419	1.021	0.414	1.022	0.411
1.039	0.430	1.031	0.424	1.032	0.422
1.050	0.444	1.049	0.445	1.042	0.435
1.060	0.469			1.060	0.455
1.070	0.470			1.078	0.470
1.089	0.490	1.088	0.491		
1.109	0.526				

HBF

FIG. I (a)
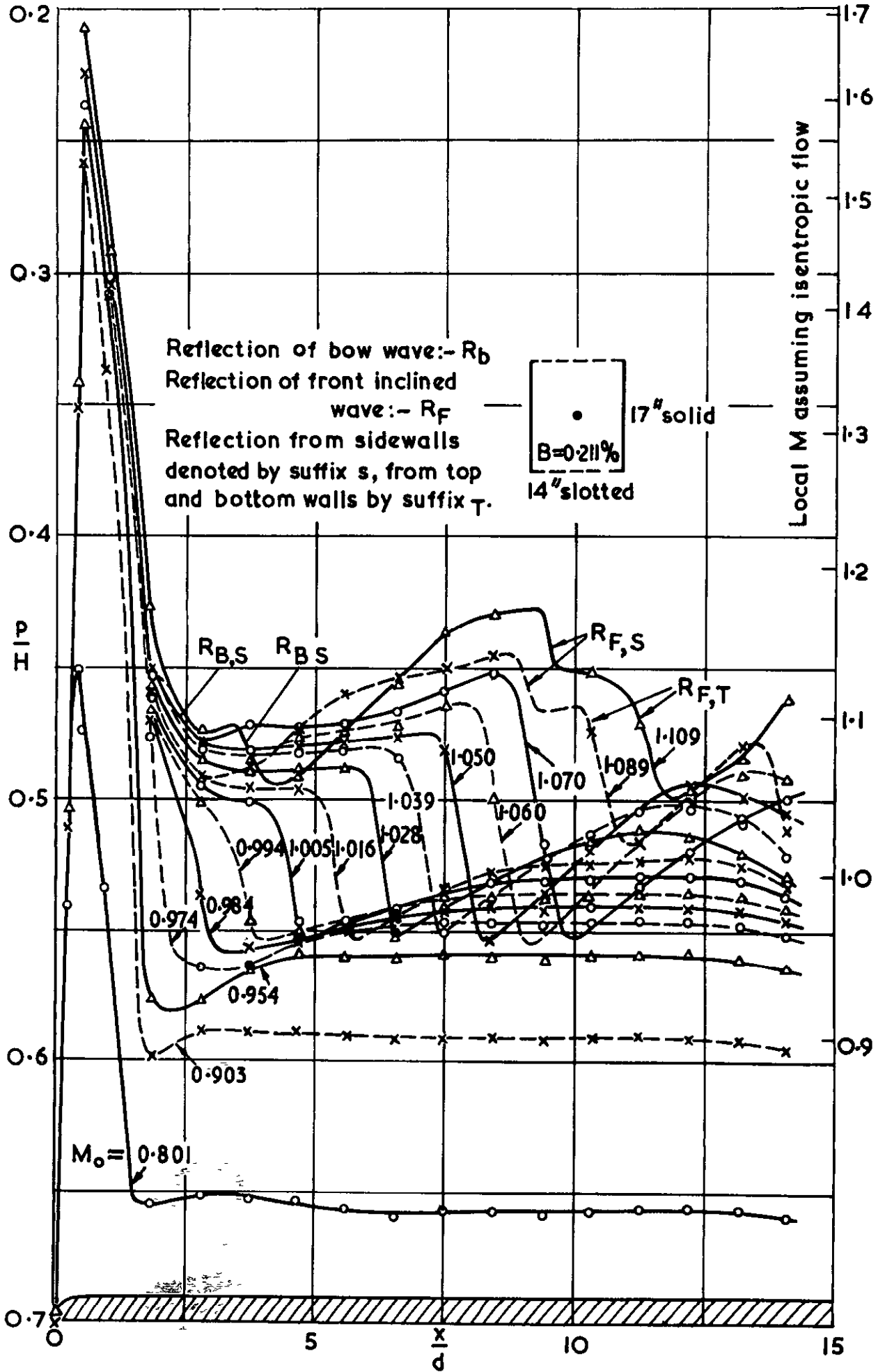
Pressure distribution on hemisphere–cylinder body in 17″× 14″ tunnel

FIG. I.(b)
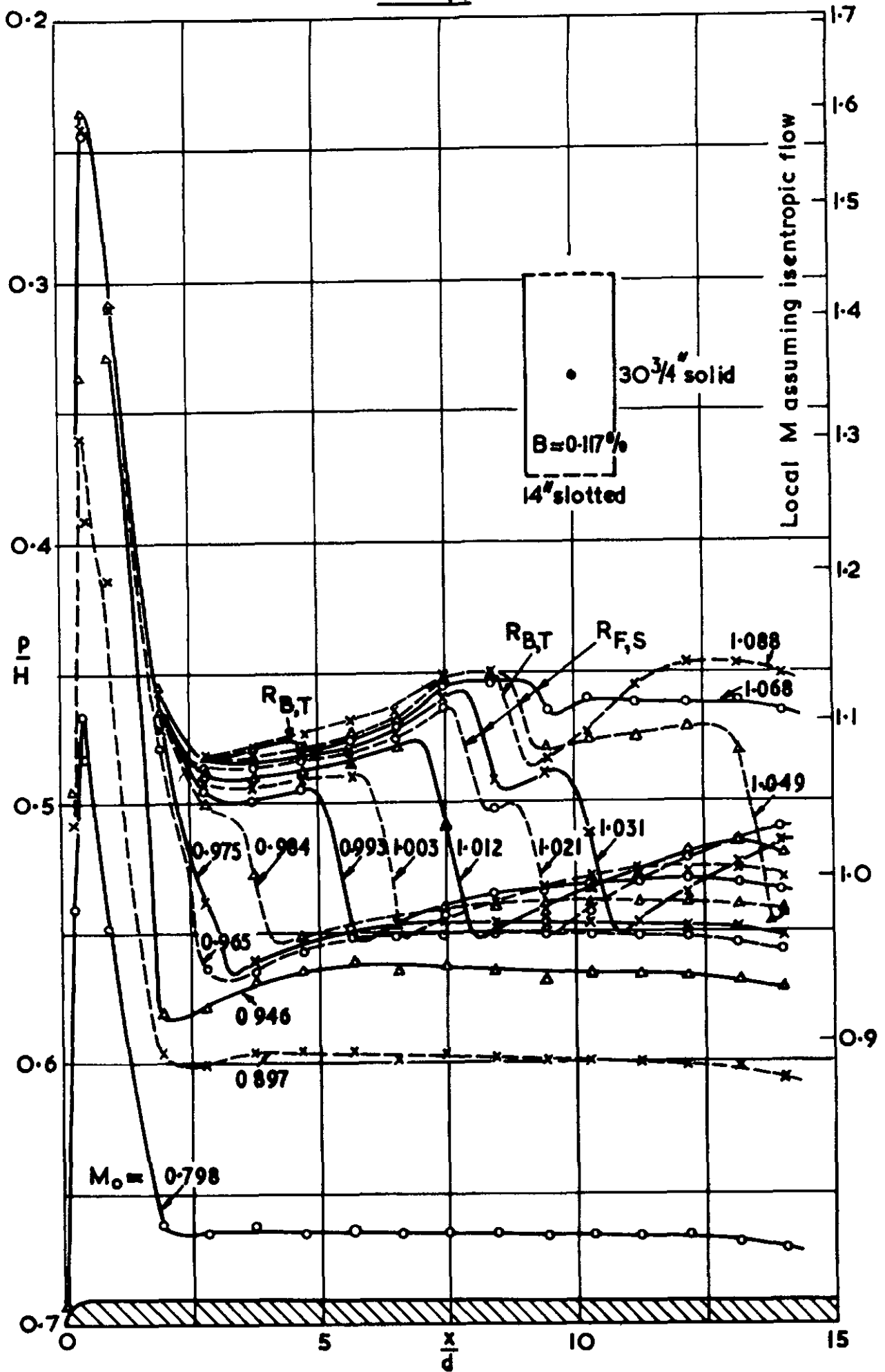
Pressure distribution on hemisphere-cylinder body in 30¾" x 14" tunnel

FIG. 1 (c)
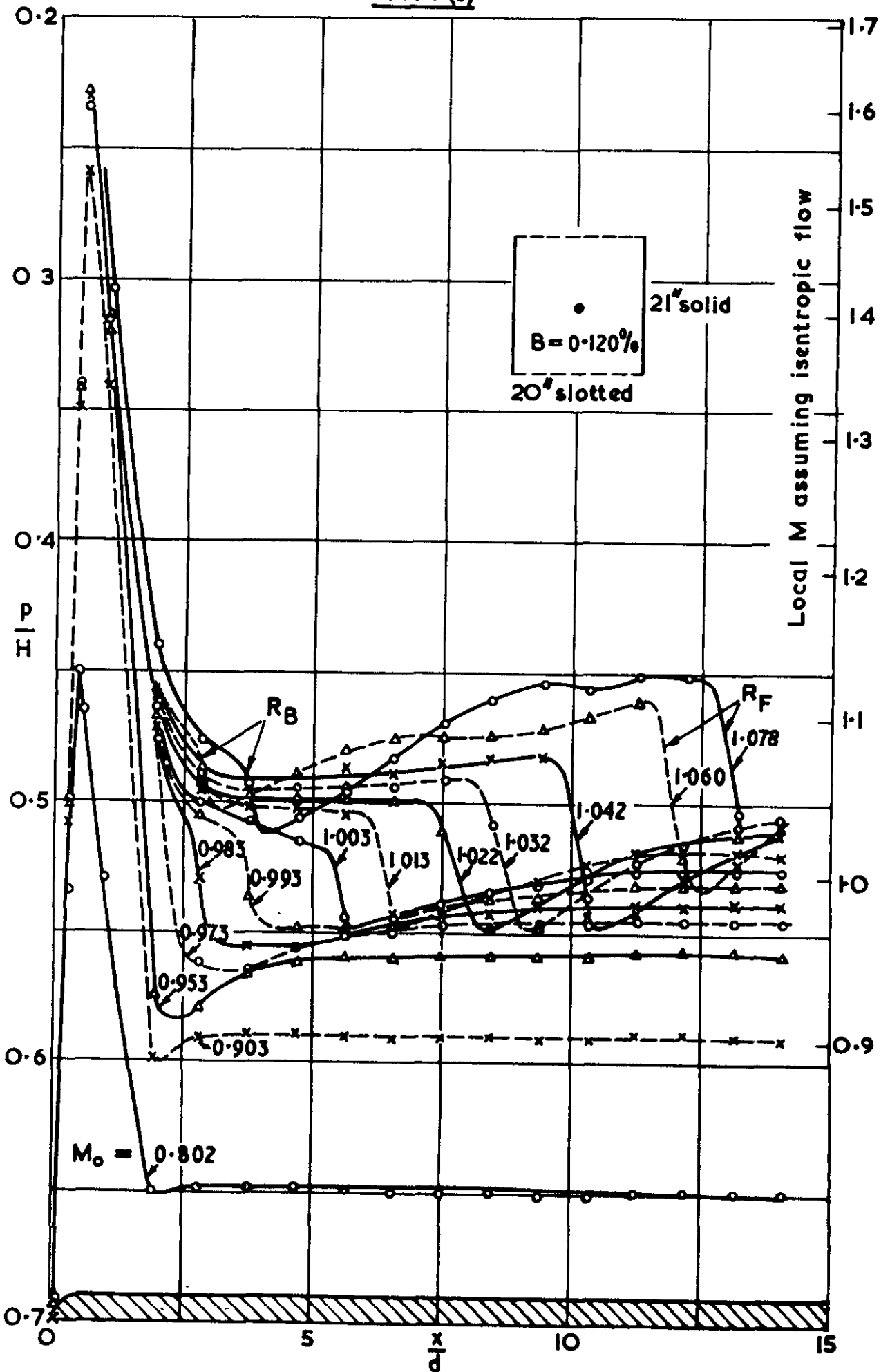
Pressure distributions on hemisphere-cylinder body in 21″ x 20″ tunnel

FIG. 2.
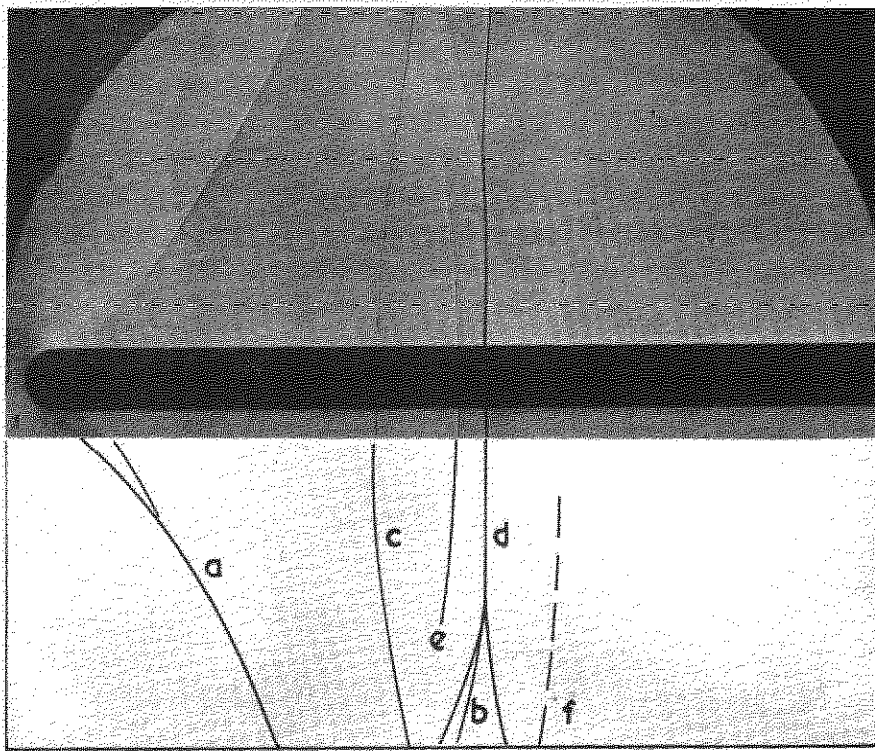
Key:—

a: front inclined shock.

b: reflection of 'a' from slotted wall.

c: intersection of 'a' with glass sidewall.

d: terminal shock.

e: effect of reflection of 'a' from sidewall.

f: reflection of 'd' from slotted wall.

N.B. The trace 'e' does not correspond to a normal shock at the model position but at some station between the wall and the model.
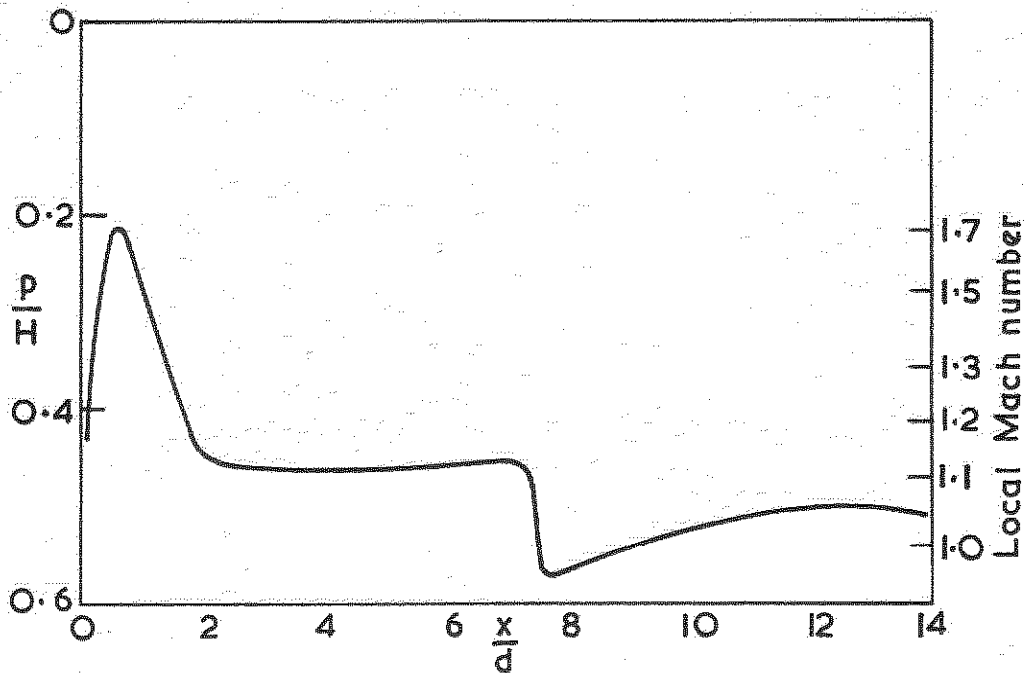
Typical flow pattern and pressure distribution at $M_o = 1 \cdot 050$ in 17 in. x 14 in tunnel

FIG.3 (a)
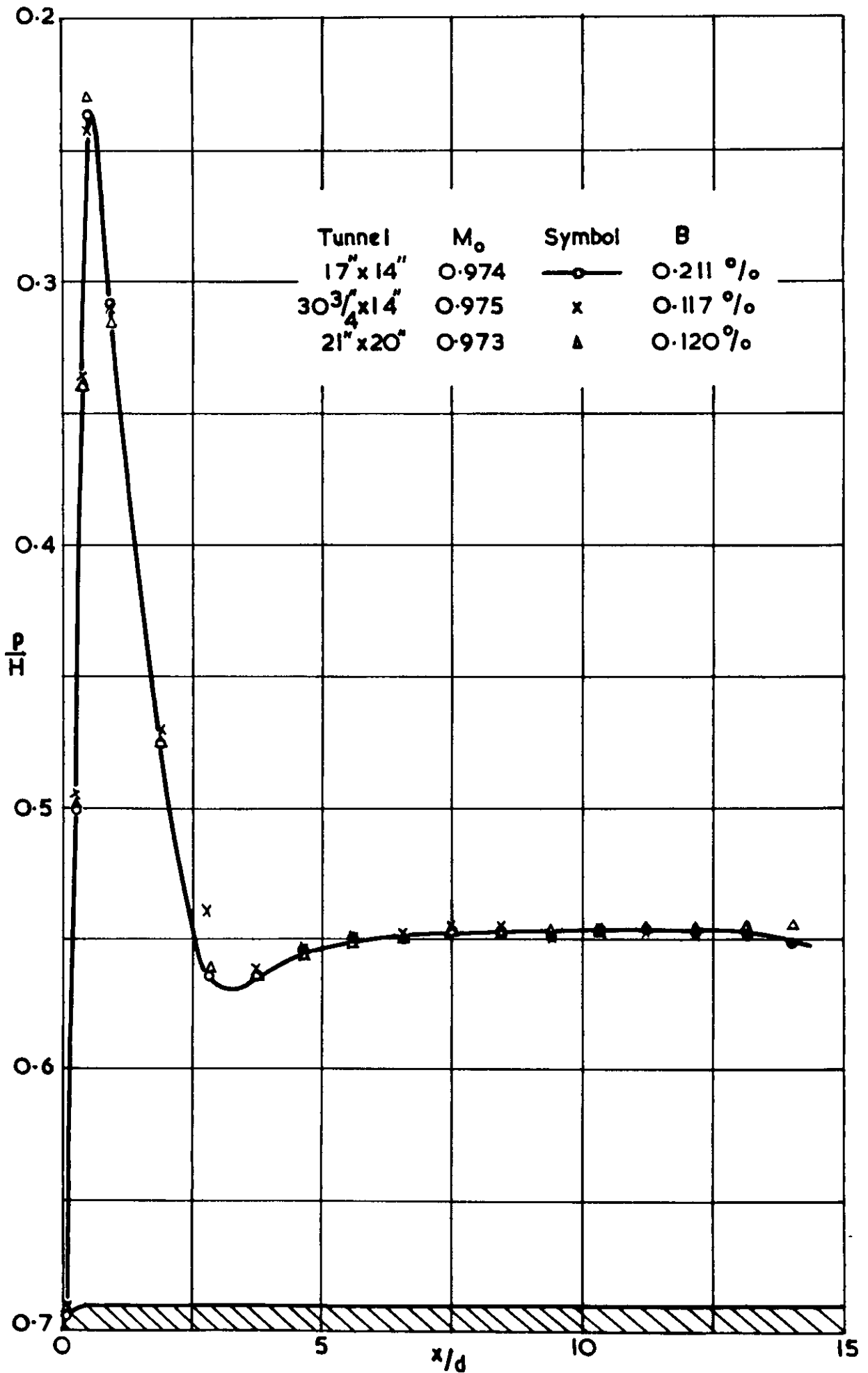
Pressure distributions on hemisphere — cylinder body near M₀=0·974.

FIG. 3 (b.)

Tunnel	M_0	Symbol	B
17"x 14"	1·005	——o——	0·211 %
30¾"x 14"	1·003	----x----	0·117 %
21"x20"	1·003	—·—▲—·—	0·120 %
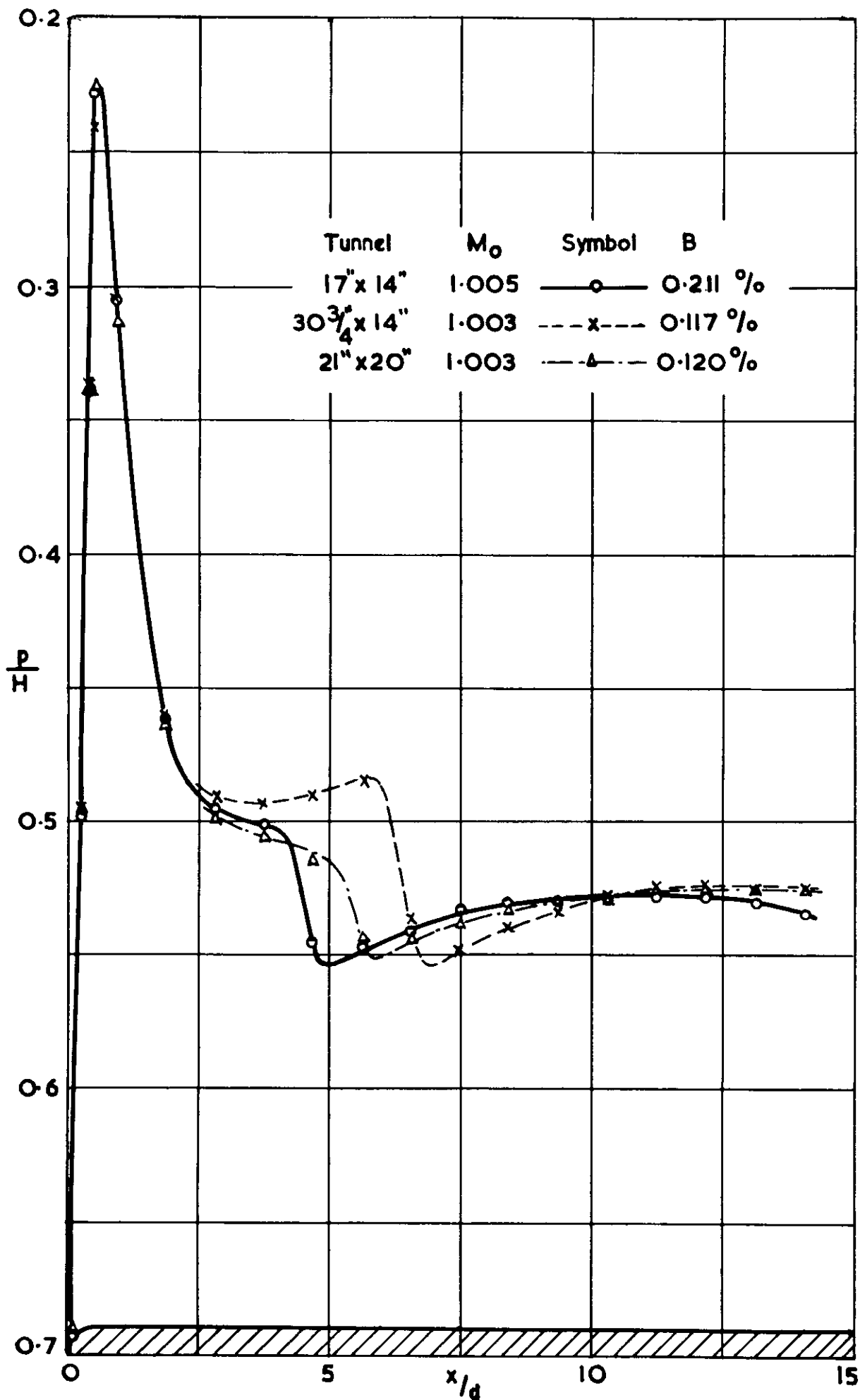
Pressure distributions on hemisphere — cylinder body near M = 1·003.

FIG. 3.(c.)
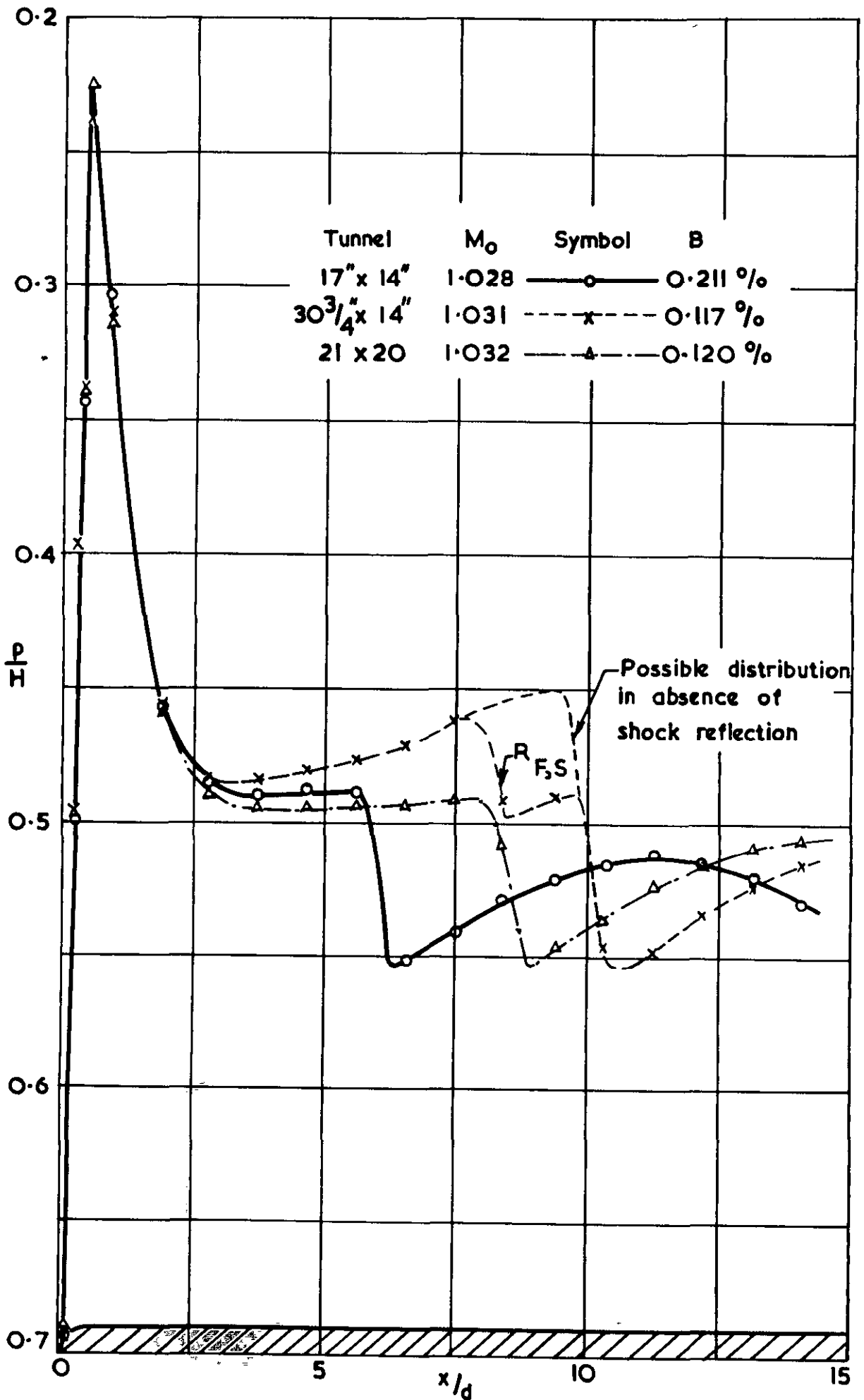
Tunnel	M_O	Symbol	B
17″x 14″	1·028	——o——	0·211 %
30³/₄″x 14″	1·031	----x----	0·117 %
21 x 20	1·032	—·—▲—·—	0·120 %

Possible distribution
in absence of
shock reflection

$R_{F_3}S$

$\frac{p}{H}$

x/d

Pressure distributions on hemisphere — cylinder body near $M_O = 1·030$.

FIG.3.(d.)

Tunnel	M_o	Symbol	B
17"x 14"	1·050	———o———	0·211 %
30¾"x14"	1·049	---x---	0· 117 %
21"x20"	1·042	—·—▵—·—	0·120 %
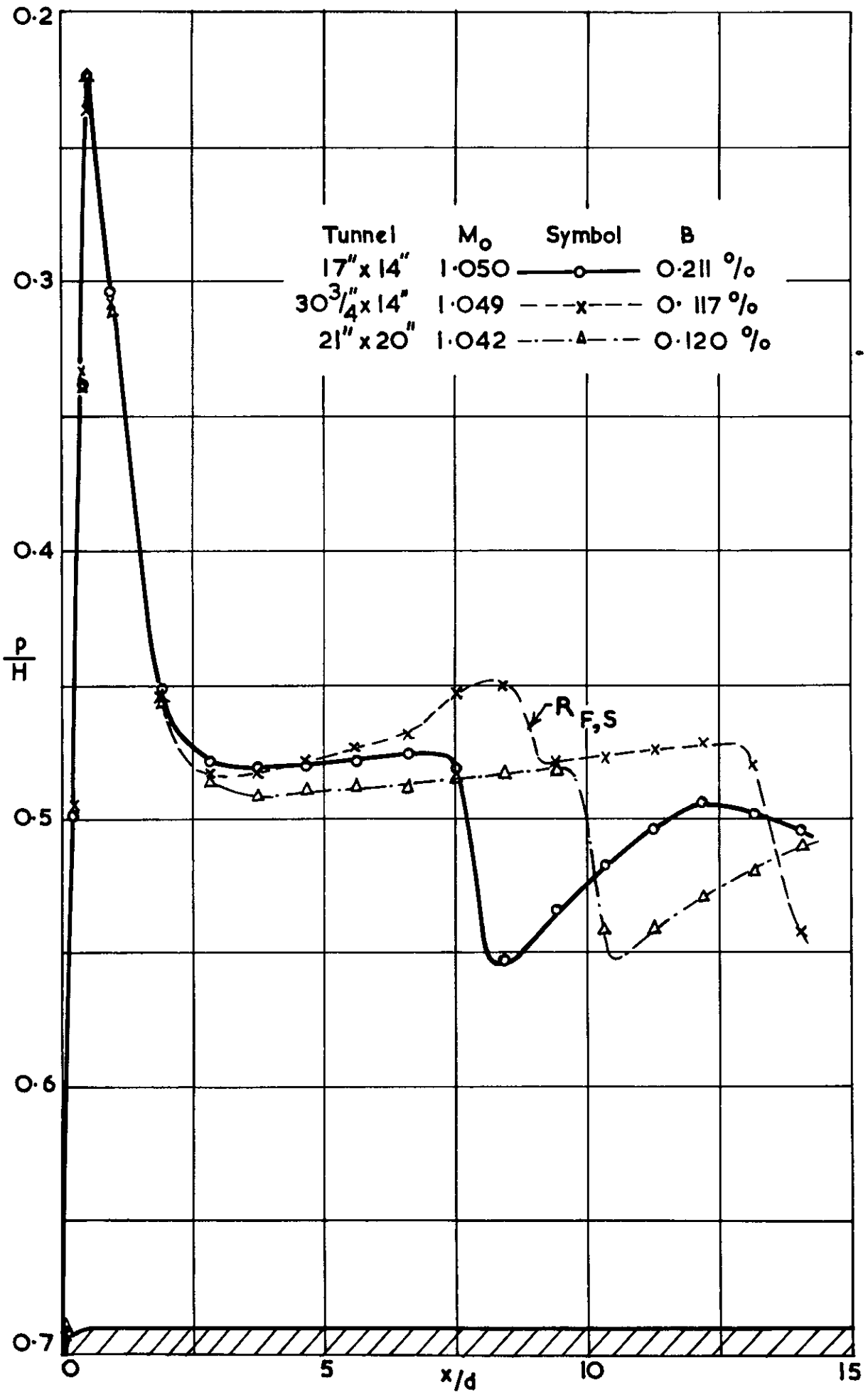
Pressure distributions on hemisphere — cylinder body near M = 1·045.

FIG.3.(e.)

Tunnel	M_O	Symbol	B
17"x 14"	1·050	——o——	0·211 %
30 3/4" x 14"	1·012	----x----	0·117 %
21"x 20"	1·022	—·—△—·—	0·120 %
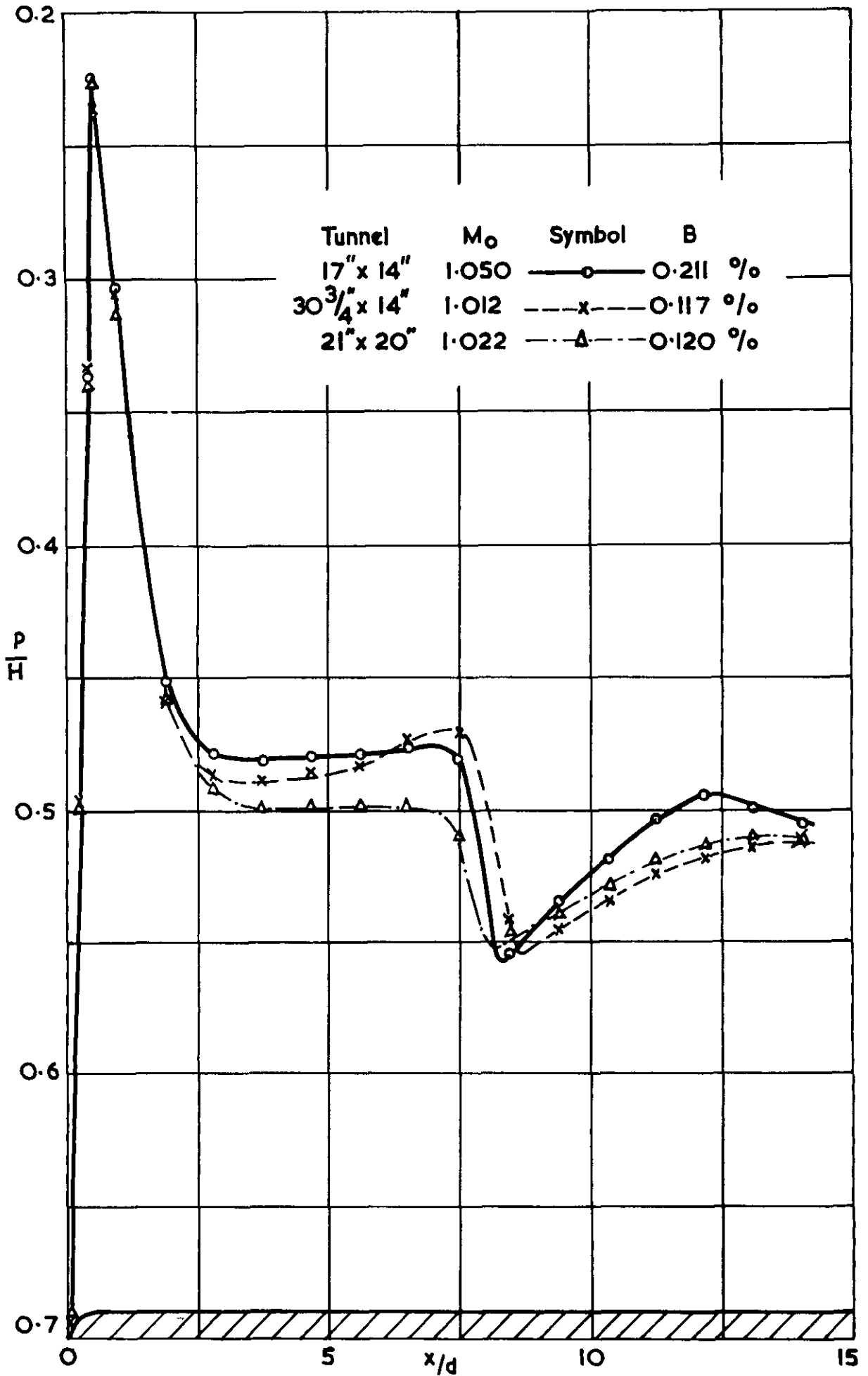
Pressure distributions on hemisphere – cylinder model at approximately constant shock position.

FIG. 4.

N.B. Plain symbols denote results from Schlieren photographs; flagged symbols denote shock position deduced from pressure distributions.

Tunnel	Symbol	B
30³/₄ in. x 14 in.	—x — —	0·117 %
21 in. x 20 in.	— ·Δ— ·—	0·120 %
17 in. x 14 in.	⌐—o————	0·211 %
	•	0·204 % ⎱ Ref 2
	————	0·002 % ⎰
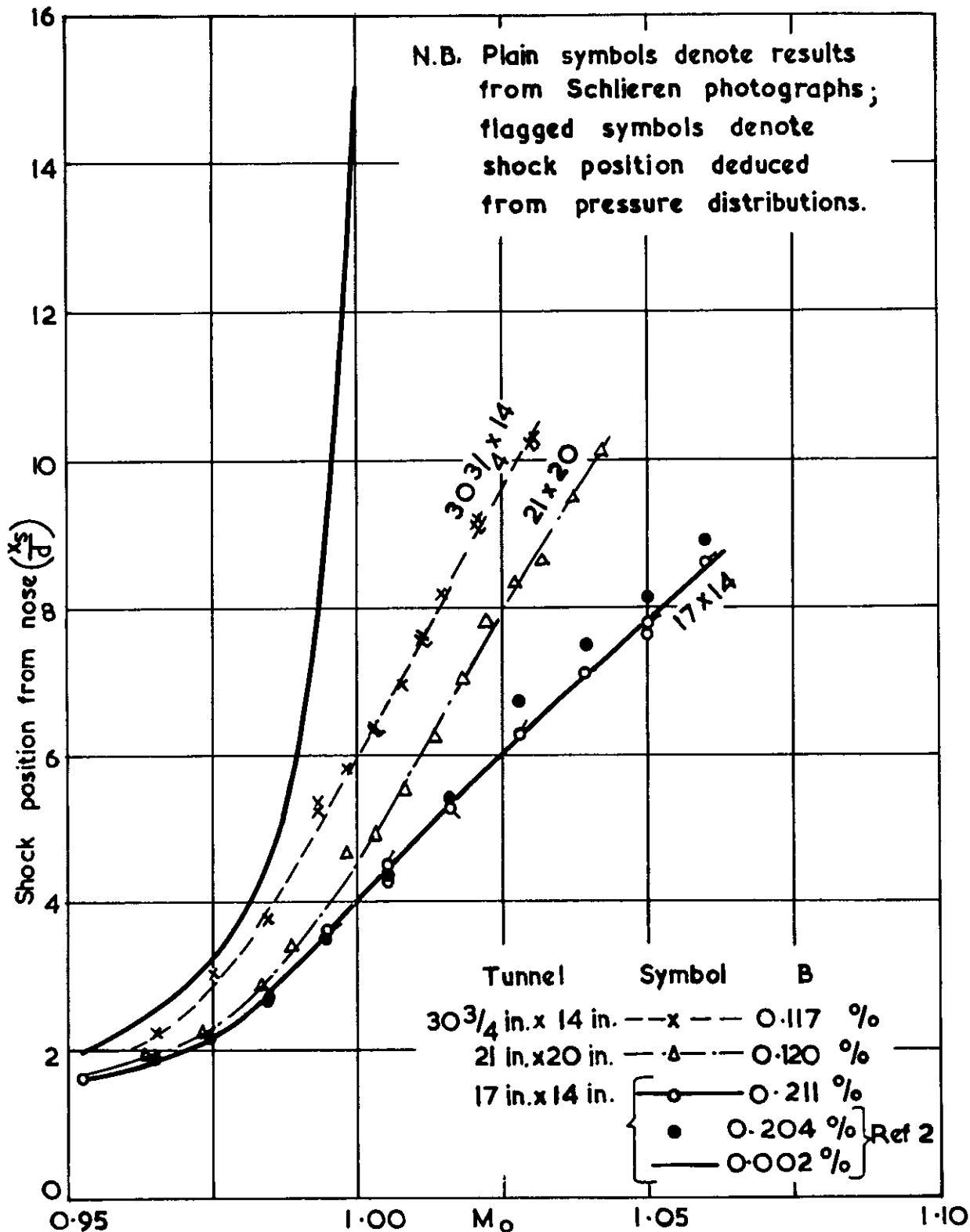
Effect of blockage ratio on terminal shock position.

FIG 5 (a & b)
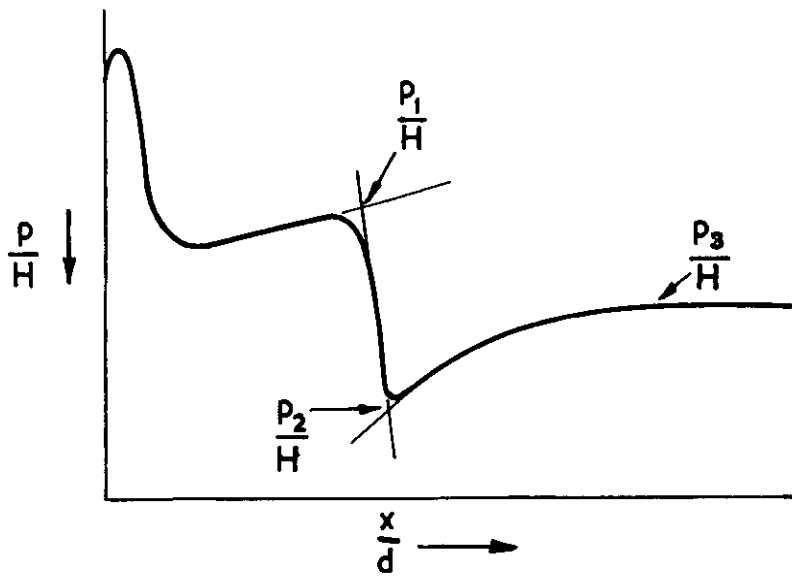
(a): Definition of specific pressure ratios occuring in distribution

Tunnel	Symbol	B
17in. x 14in.	o	0·211%
30¾in.x14in.	x	0·117%
21in. x 20in.	△	0·120%

Static pressure ratio corresponding to M_0

Local Mach number, assuming isentropic flow

Corrected stream Mach number, M_0
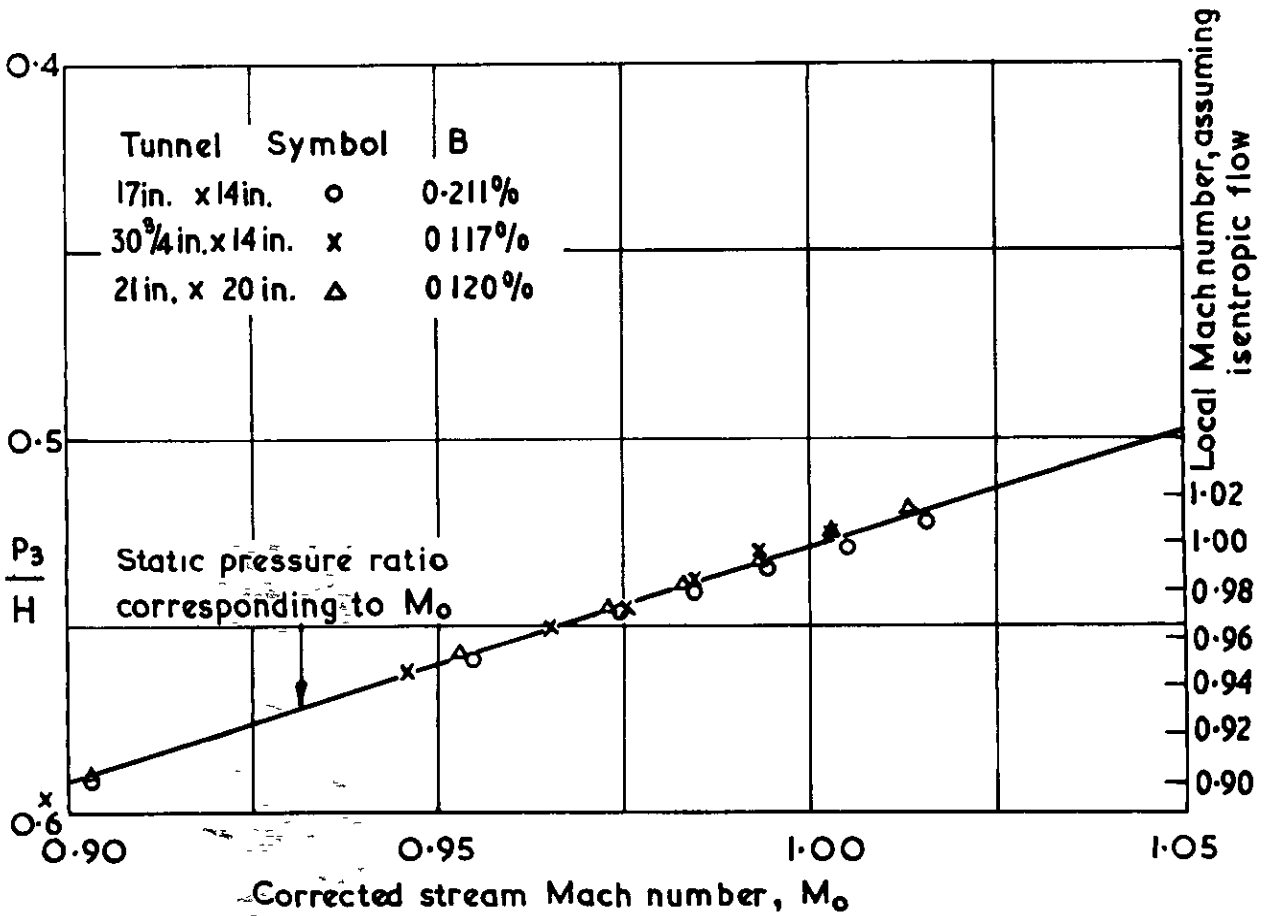
(b) Variation of estimated downstream pressure ratio $\left(\dfrac{P_3}{H}\right)$ with corrected stream Mach number

FIG. 5 (c)
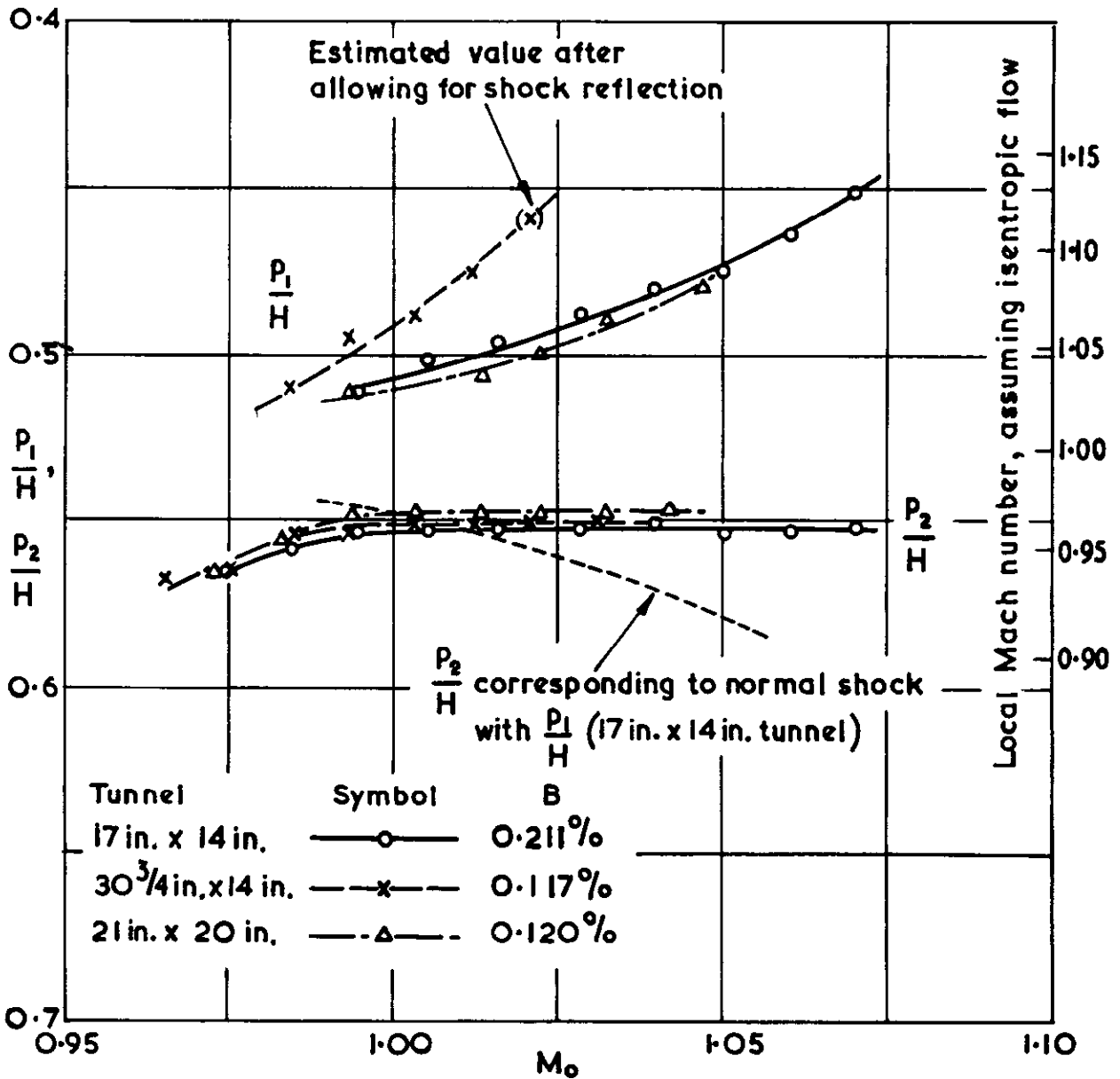
(c) Variation of estimated pressure ratios upstream and downstream of terminal shock with stream Mach number.

FIG. 6
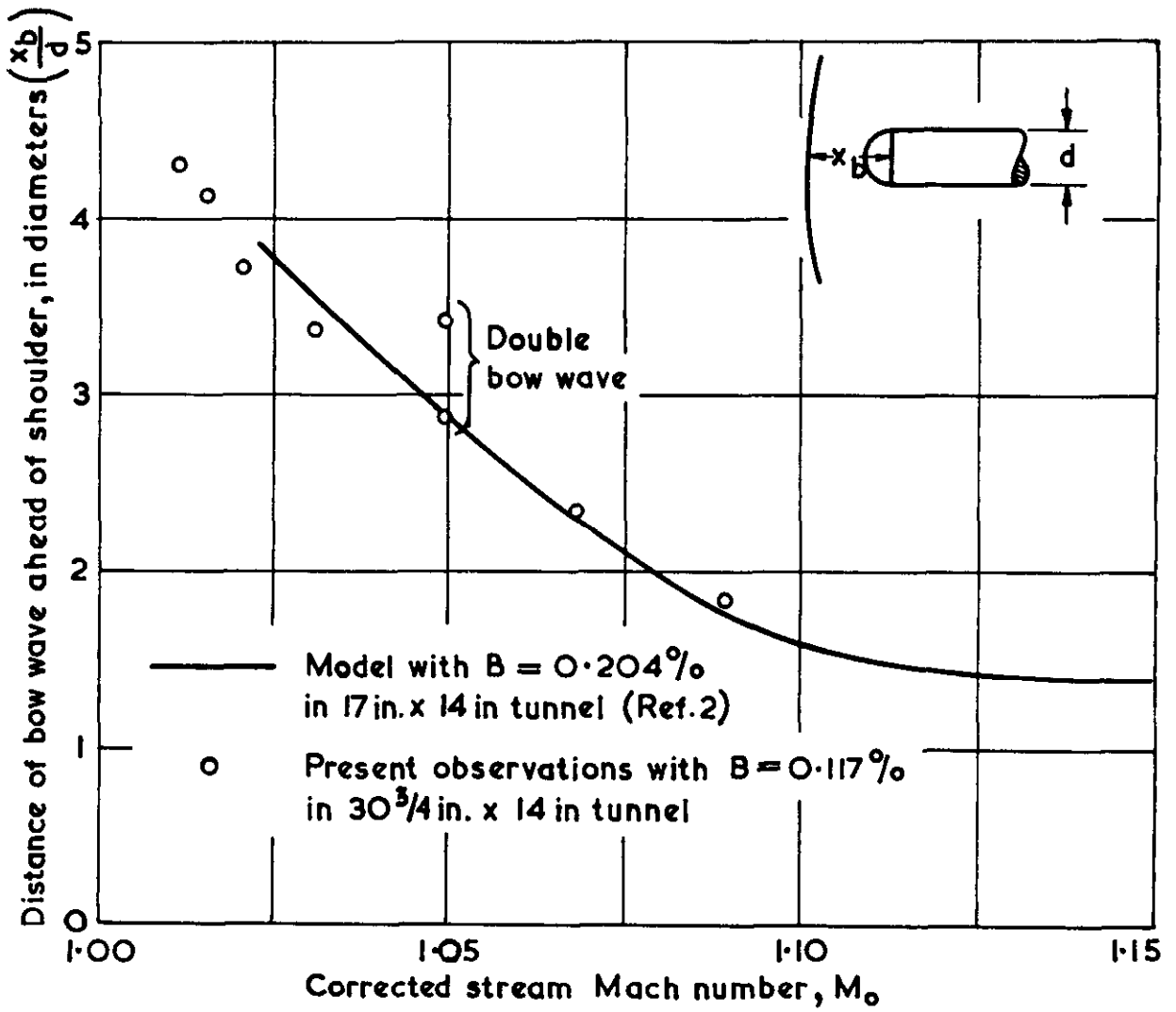
Comparison of bow wave positions in present and earlier tests on nearly similar models

FIG. 7a.
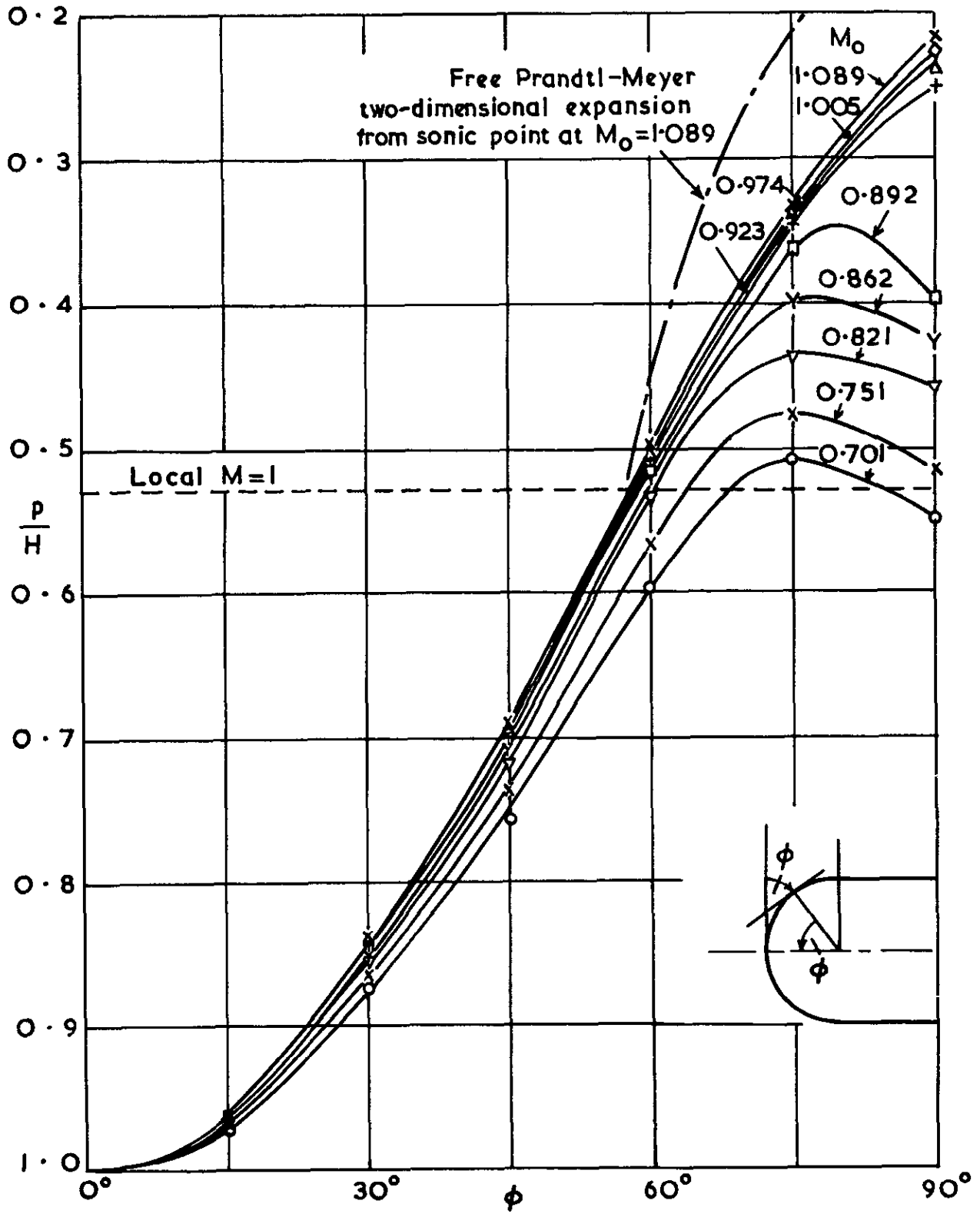
(a)   Pressure distribution around nose in 17in.x 14in.tunnel.

FIG. 7 b.
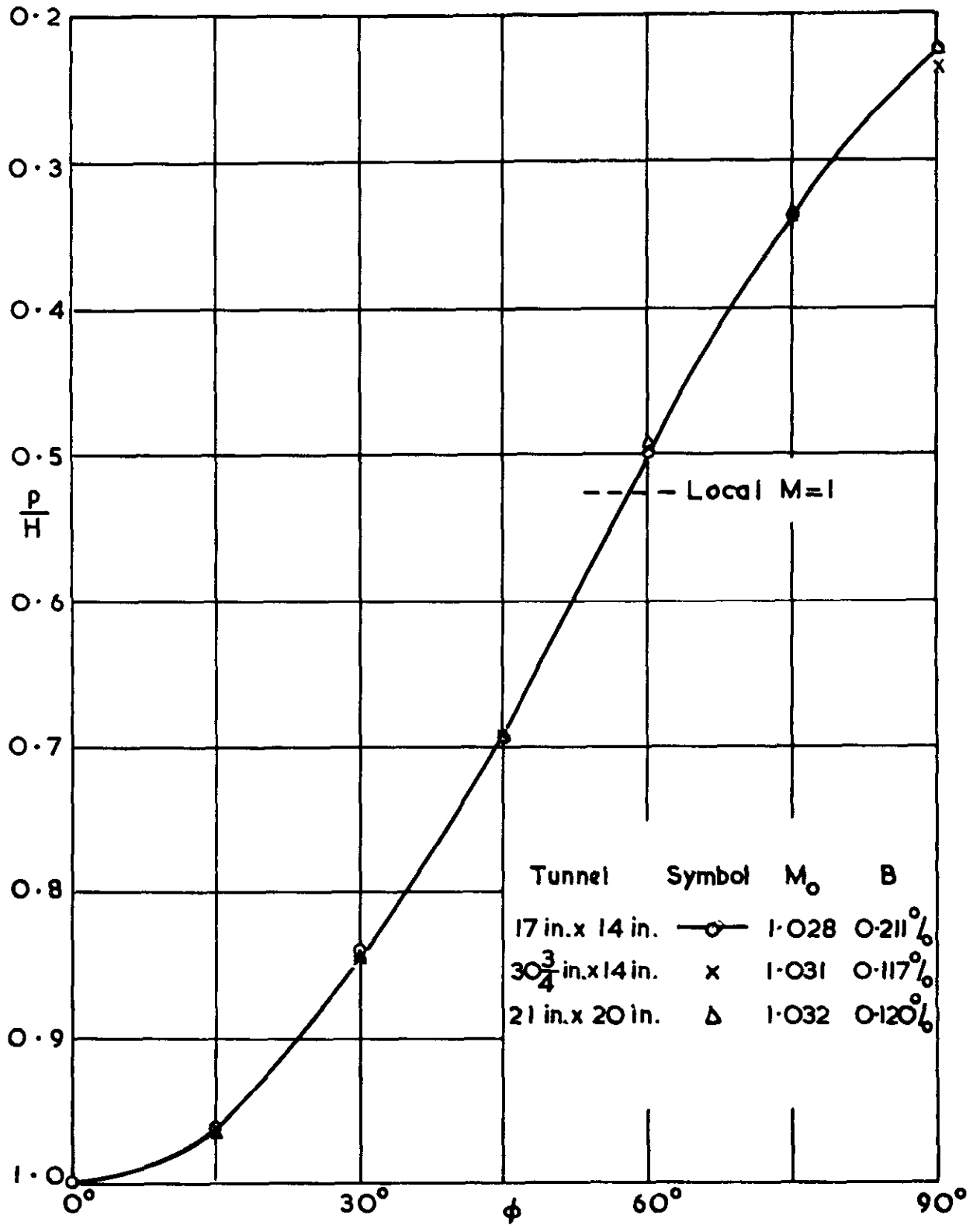
(b) Comparison of pressure distributions around nose at stream Mach numbers near 1·030.

FIG. 8.(a).
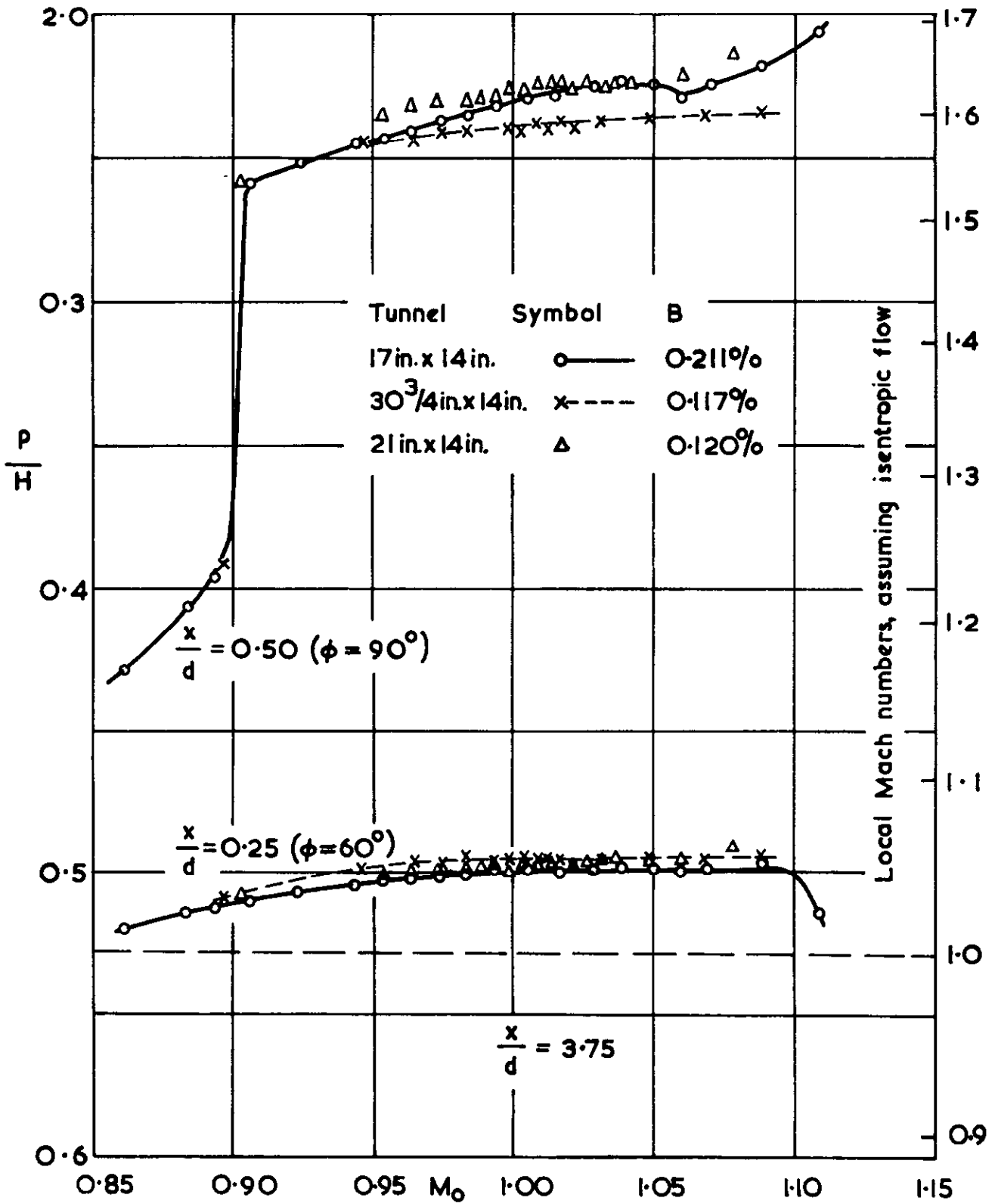
Variation of pressure at specific station on nose with stream Mach number.

FIG. 8(b.)
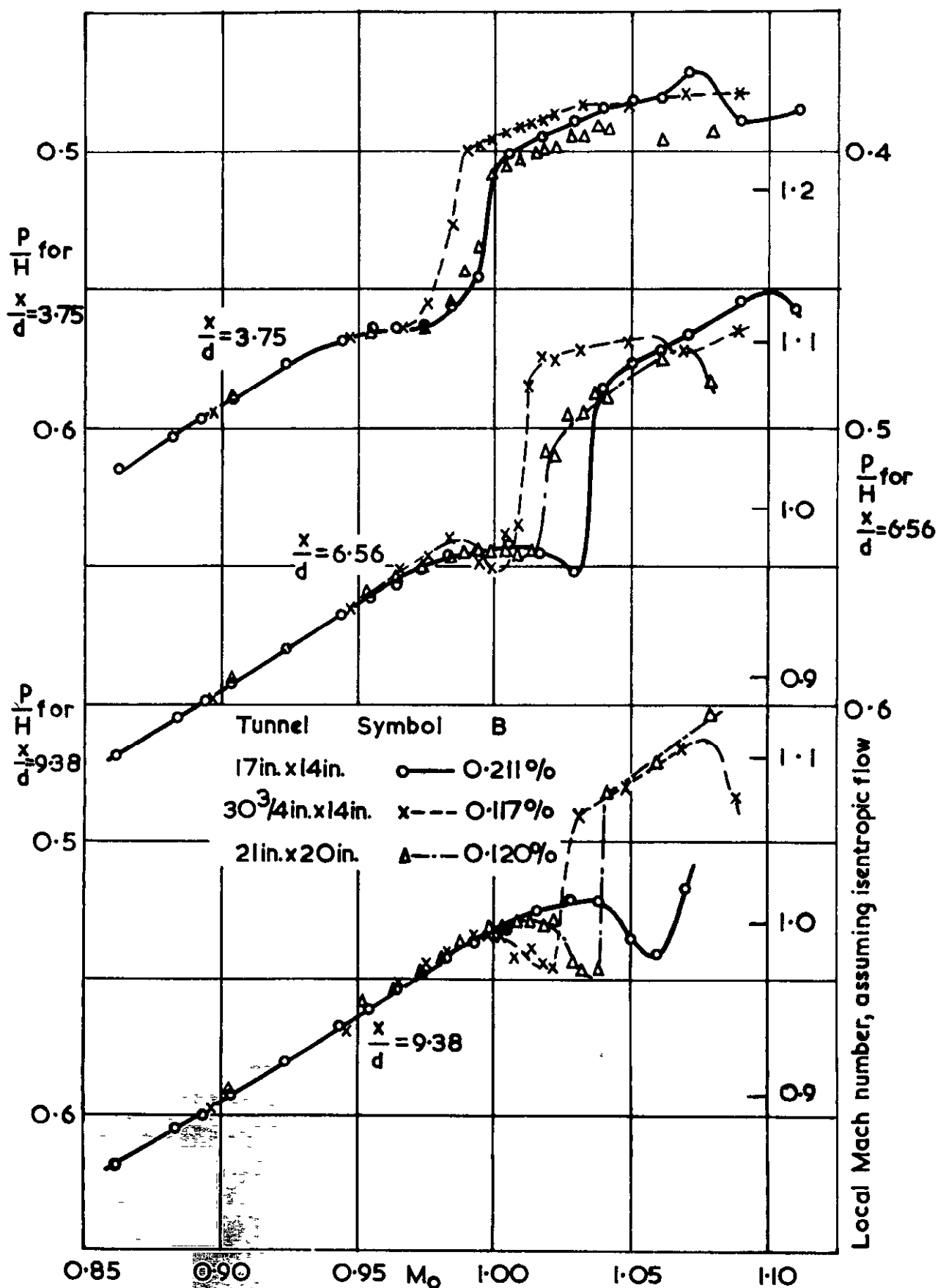
Variation of pressure at specific stations on cylinder with stream Mach number.

FIG. 9a.

Free-air sonic boundary

Disturbed sonic boundary

$M_o < 1$

Characteristics

Expansion waves — — —

Compression waves ———

Distribution with disturbed sonic boundary

$\frac{p}{H}$ ↓

Free-air distribution

$\frac{x}{d}$ →
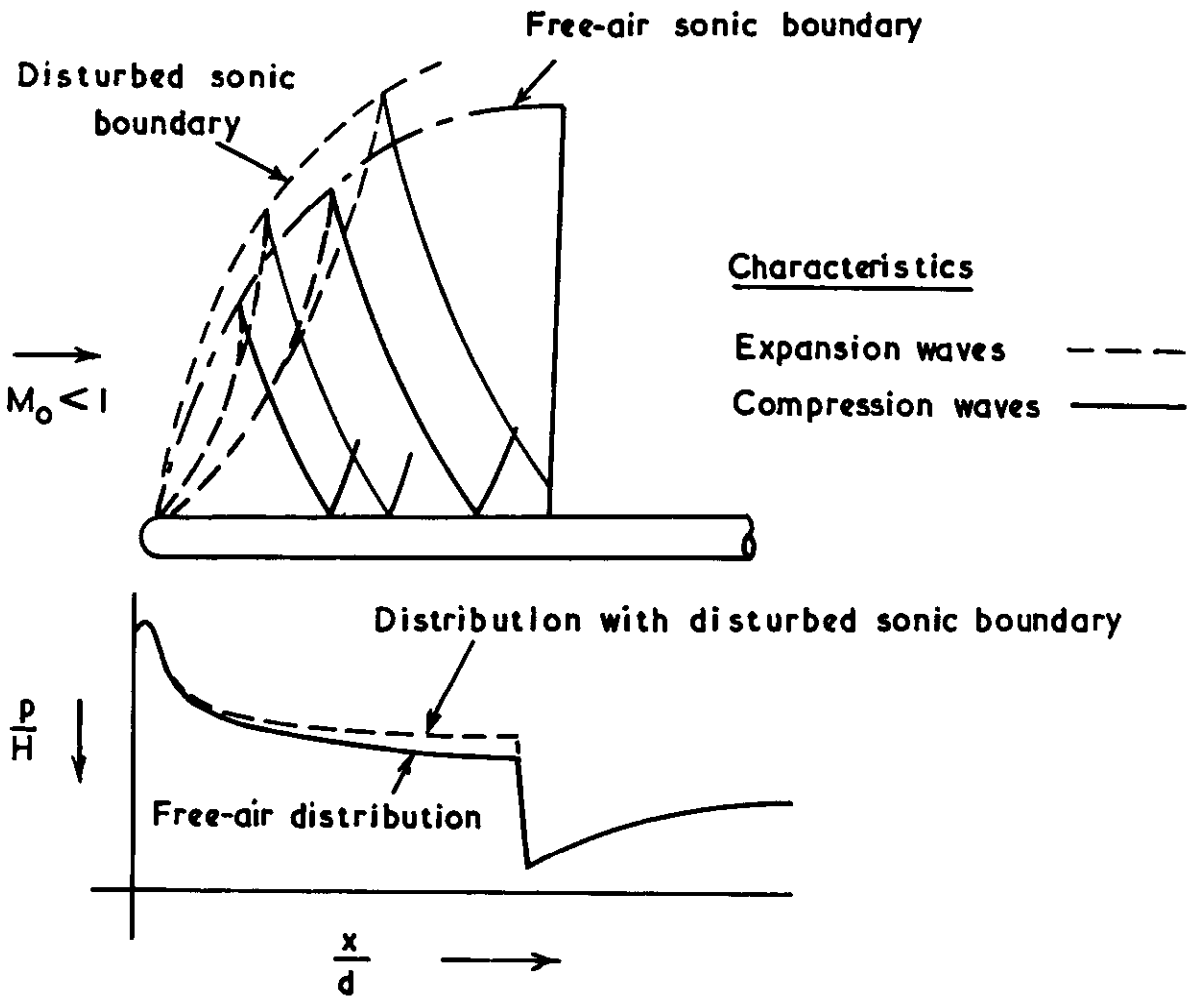
(a) Influence of disturbed sonic boundary close to partially open wall on surface pressure distribution.

FIG. 9b.

Wall at position a

Wall at position b

Sonic lines
(a, b)

$M_0 < 1$

a_3

a

b_3
b_2
a_2
b_1
a_1

$\dfrac{P}{H}$

b

a

Free-stream value

$\dfrac{x}{d}$ →

Characteristics

Expansion waves — — —

Compression waves ——————
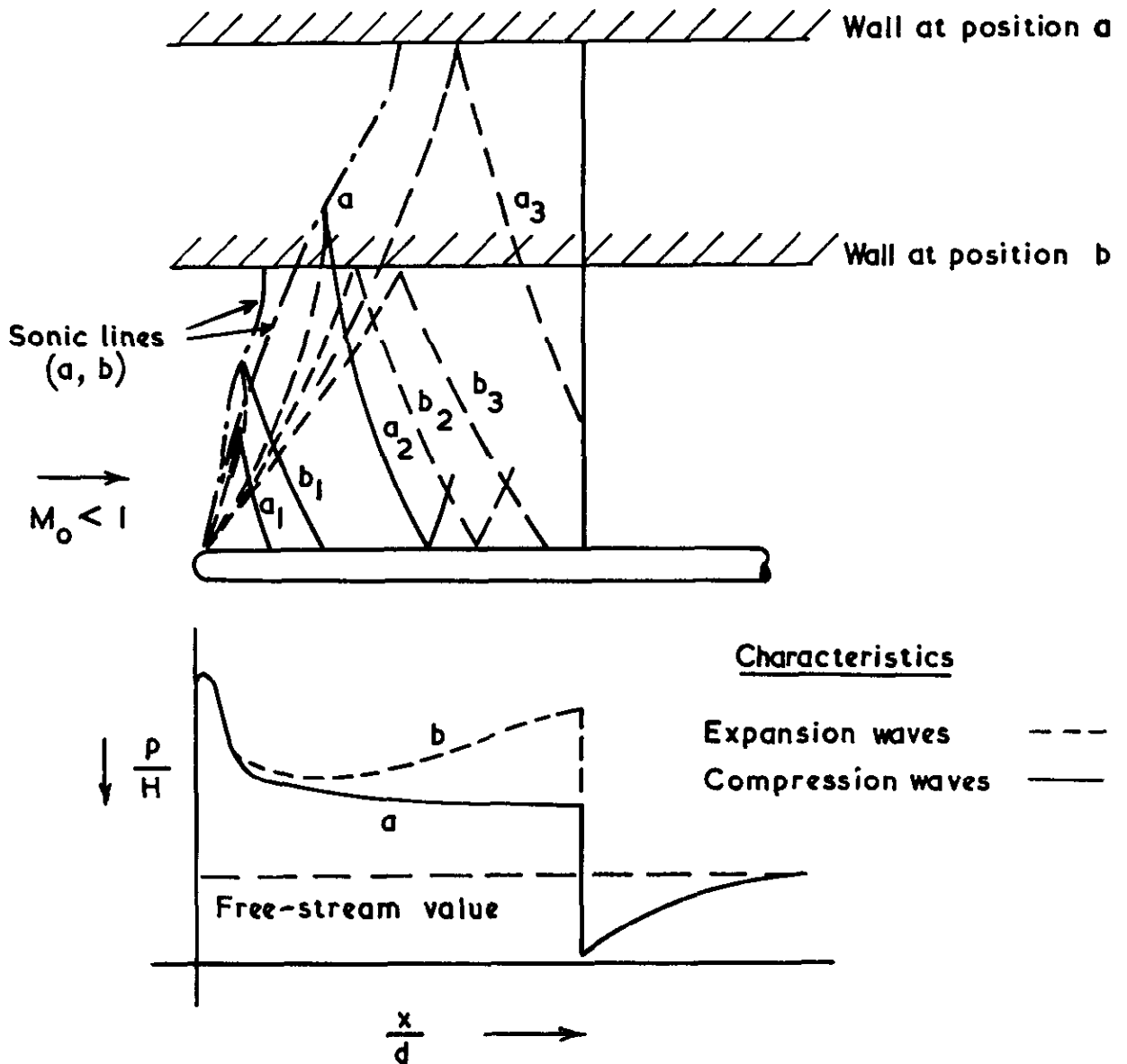
(b) Influence of solid wall position on surface
pressures at slightly subsonic stream speed.

FIG. 9c.

Wall

$M_0 > 1$

Bow wave

Sonic line

Front inclined shock
limiting influence of
reflected expansion waves
from upper wall

$\dfrac{p}{H}$

Tunnel

Free-air

Free-stream value

$\dfrac{x}{d}$
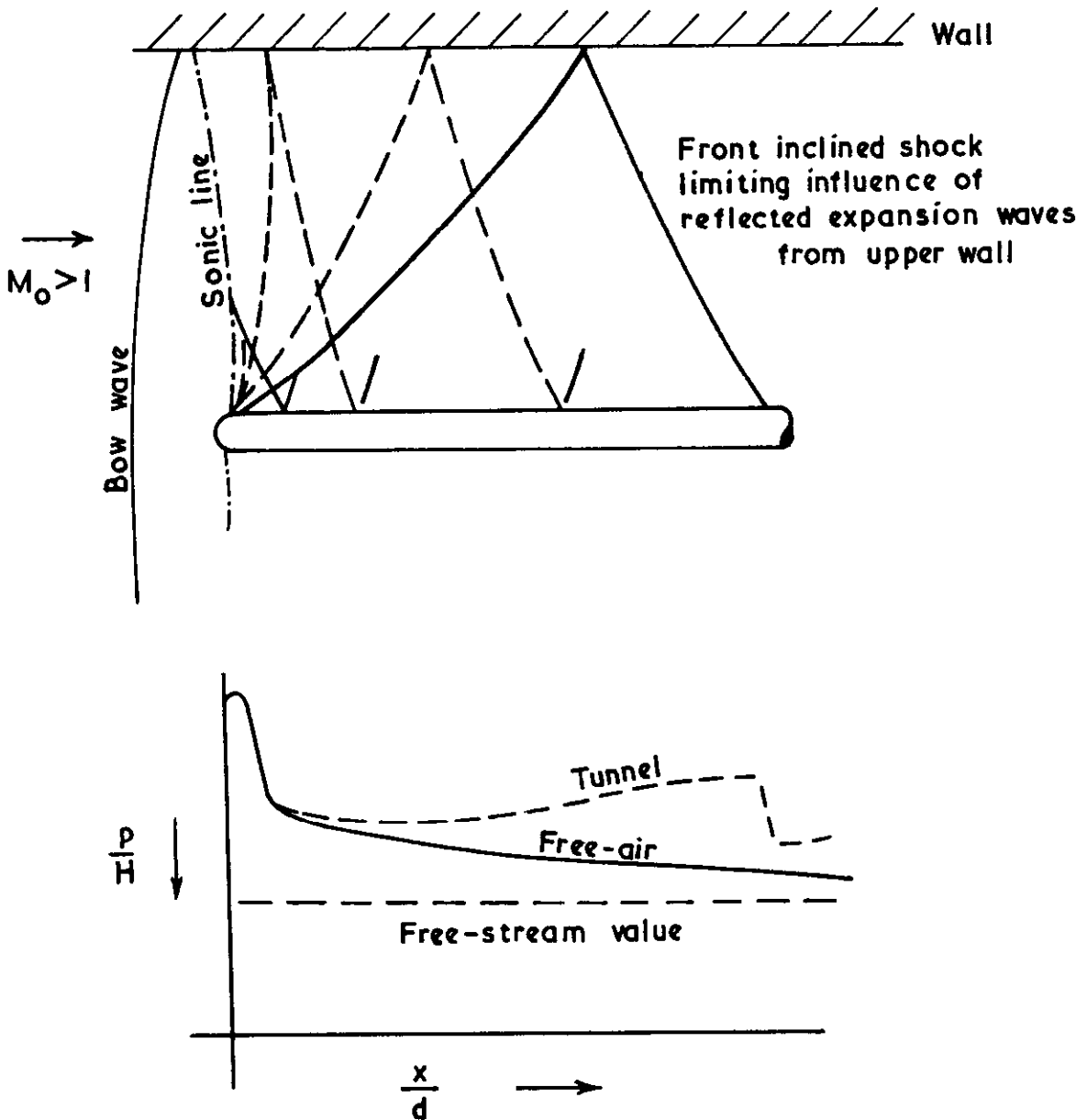
(c)   Influence of solid wall on surface pressure
distribution at slightly supersonic stream speeds.

FIG. 10a.
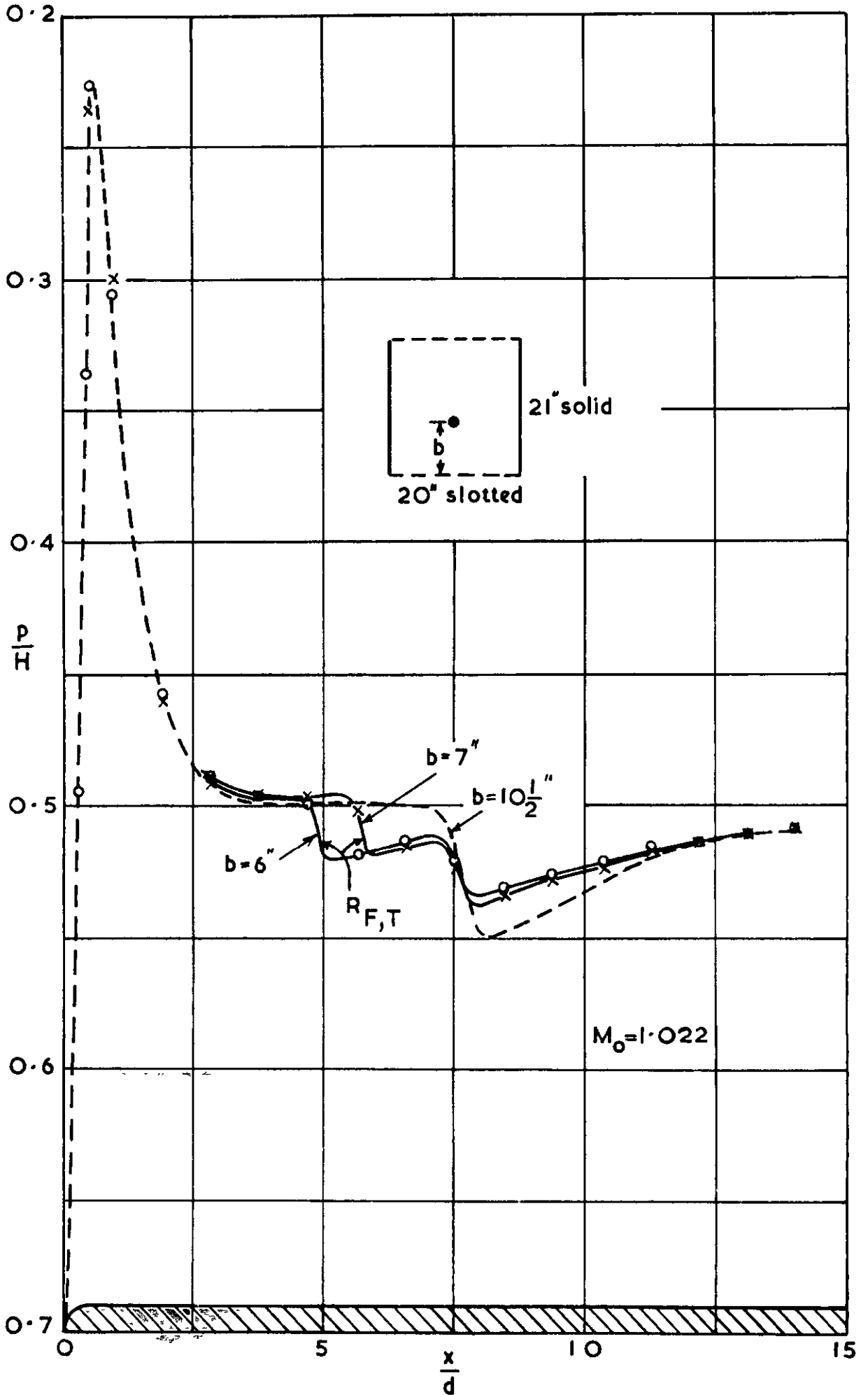
(a)   Effect of moving model towards slotted wall.

FIG. 10 b.
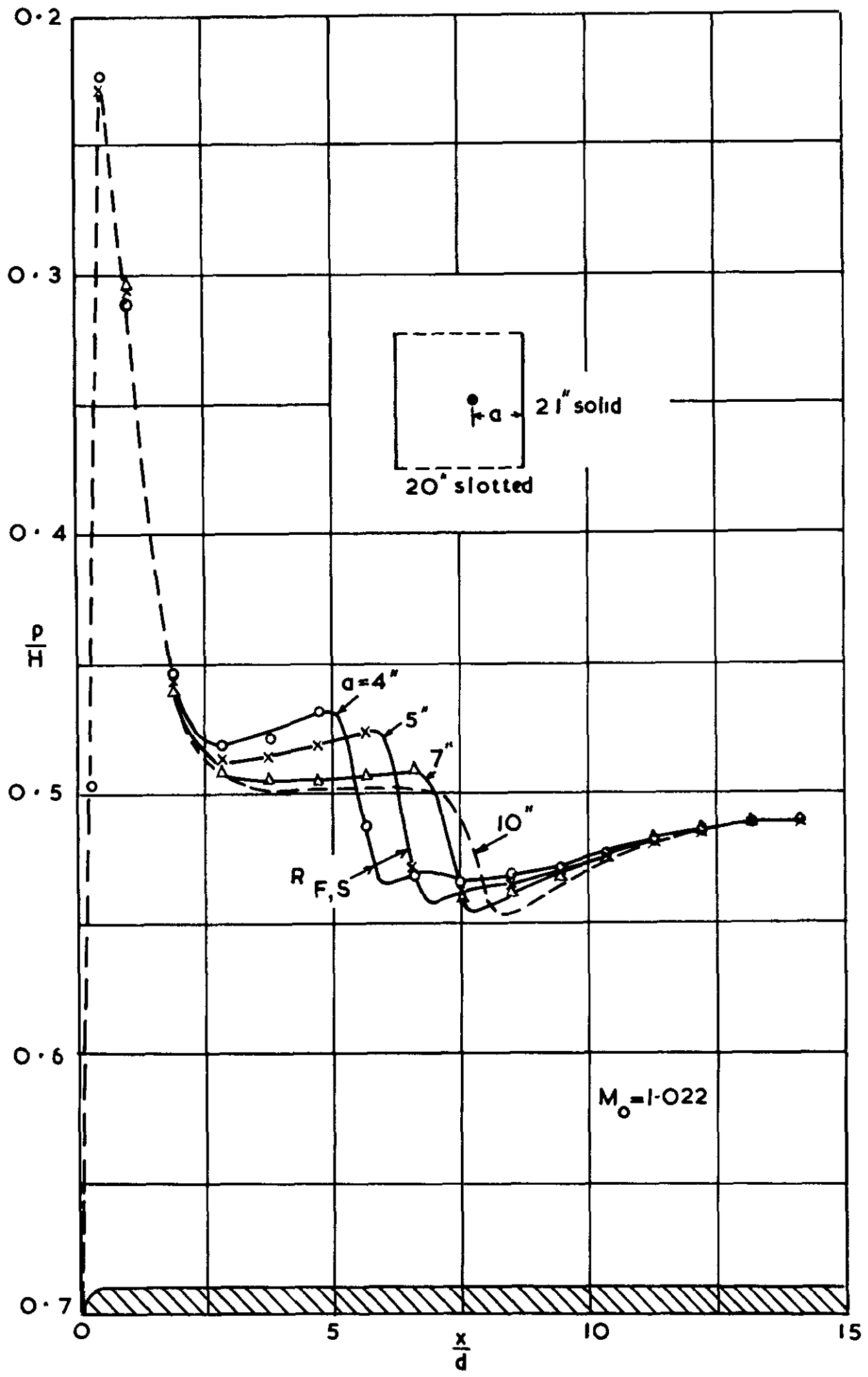
(b) Effect of moving model towards solid wall.

FIG. 11 (a & b).
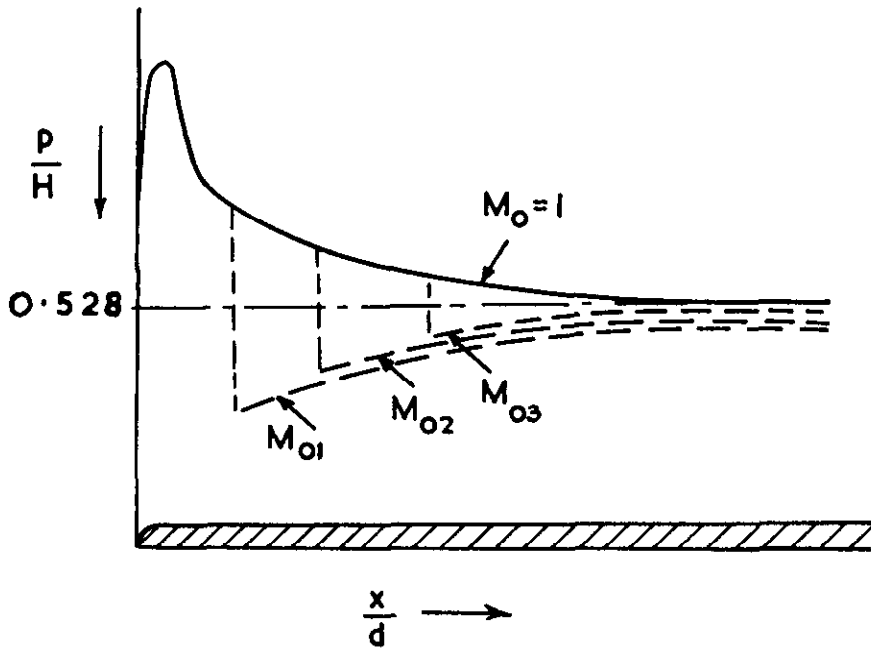
(a) **Pressure distributions near sonic stream speed in inviscid, unbounded flow.**
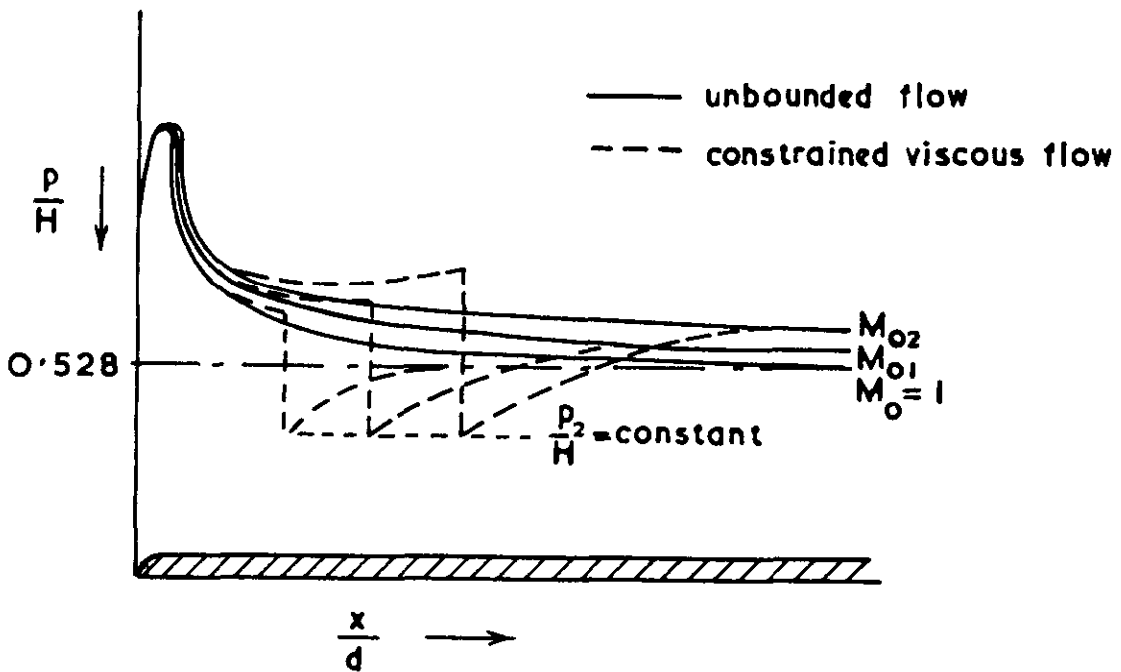
(b) **Comparison of pressure distributions just above sonic stream speed.**
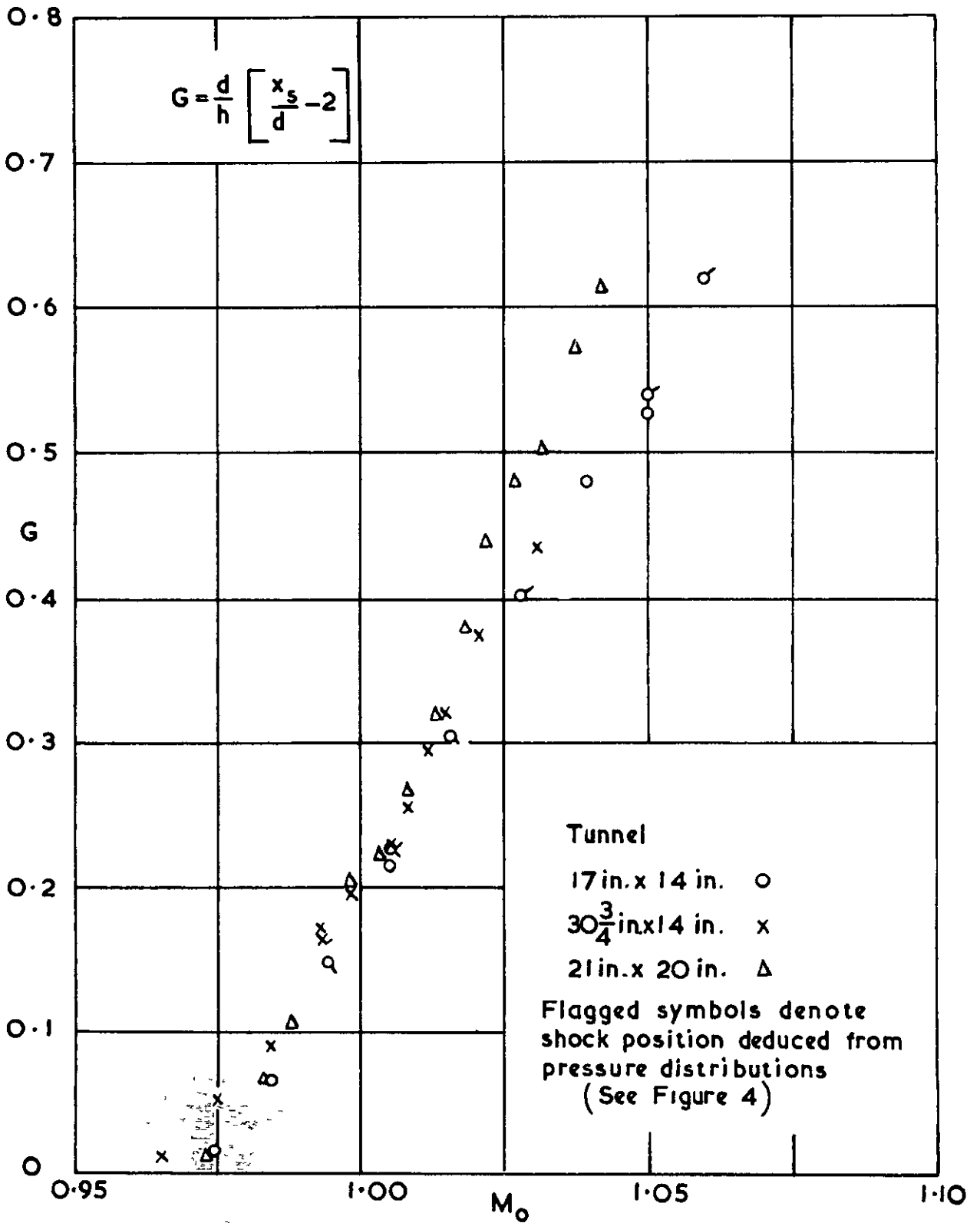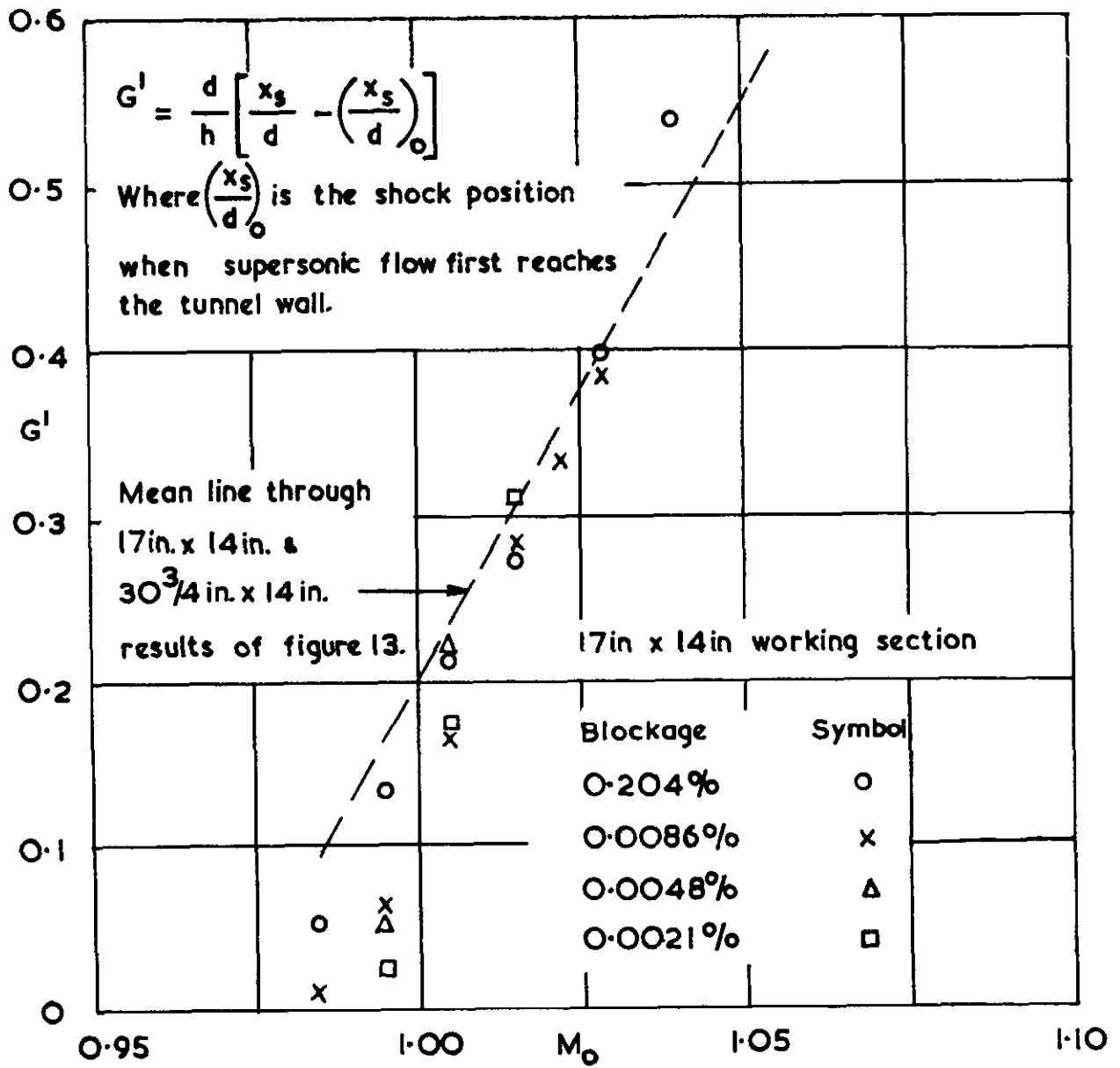
FIG. 12.

Pressure distribution on upper wall
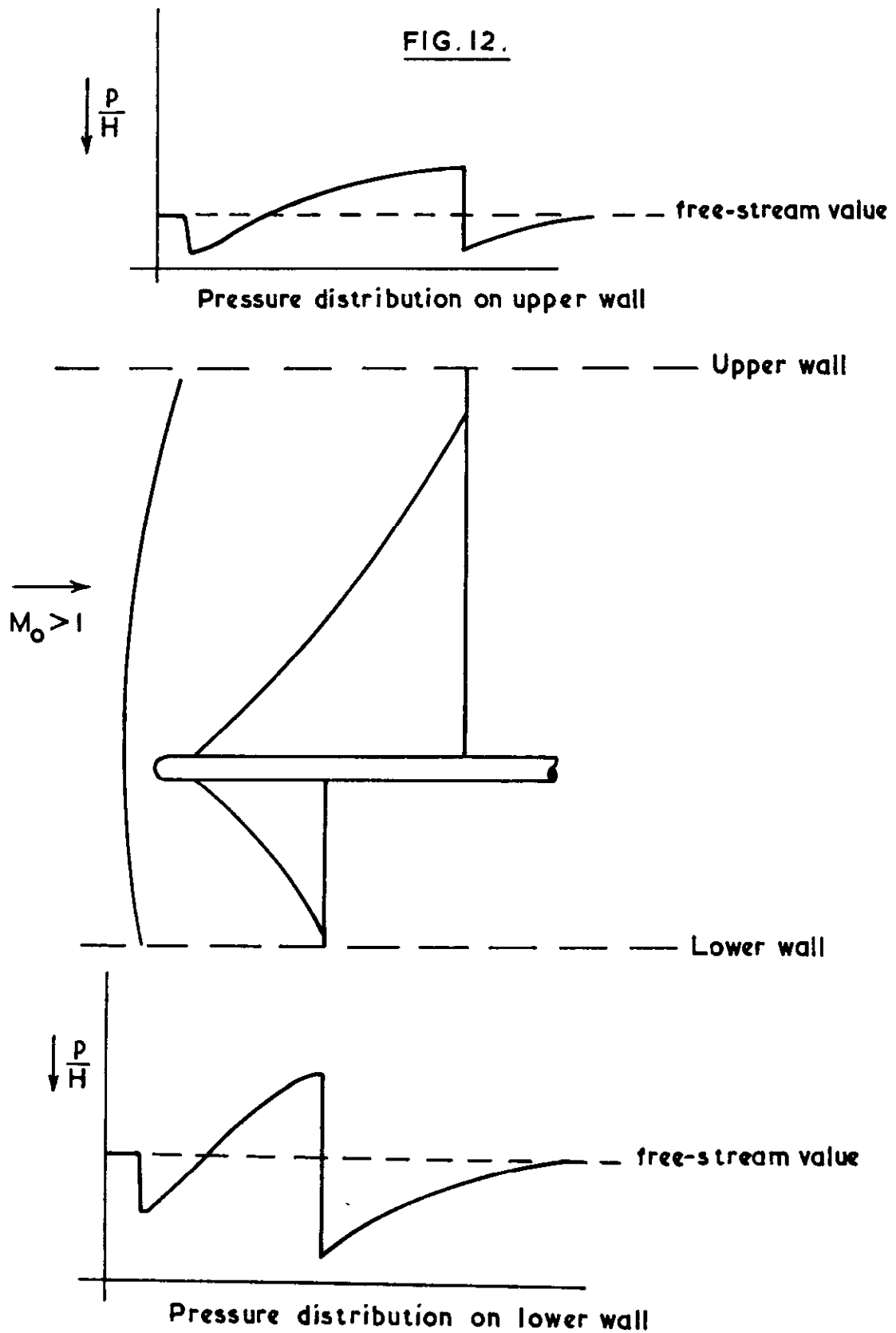
Diagram illustrating dependence of terminal shock position on shock strength at slotted wall, assuming similar pressure-recovery characteristics to rear. In real flow with off-centre model, terminal shock would not be double as drawn.

FIG. 13.

$$G = \frac{d}{h}\left[\frac{x_s}{d} - 2\right]$$

Tunnel

17 in. x 14 in.   O

$30\frac{3}{4}$ in. x 14 in.   x

21 in. x 20 in.   Δ

Flagged symbols denote
shock position deduced from
pressure distributions
(See Figure 4)

Replot of results given in Figure 4 in terms of shock-position
parameter G.

FIG. 14.

$$G^{I} = \frac{d}{h}\left[\frac{x_s}{d} - \left(\frac{x_s}{d}\right)_o\right]$$

Where $\left(\dfrac{x_s}{d}\right)_o$ is the shock position

when supersonic flow first reaches the tunnel wall.

Mean line through 17 in. x 14 in. & 30³⁄4 in. x 14 in. results of figure 13.

17 in x 14 in working section

Blockage	Symbol
0·204%	O
0·0086%	x
0·0048%	Δ
0·0021%	□

Replot of shock positions given in reference 2 for hemisphere-cylinder models of different sizes
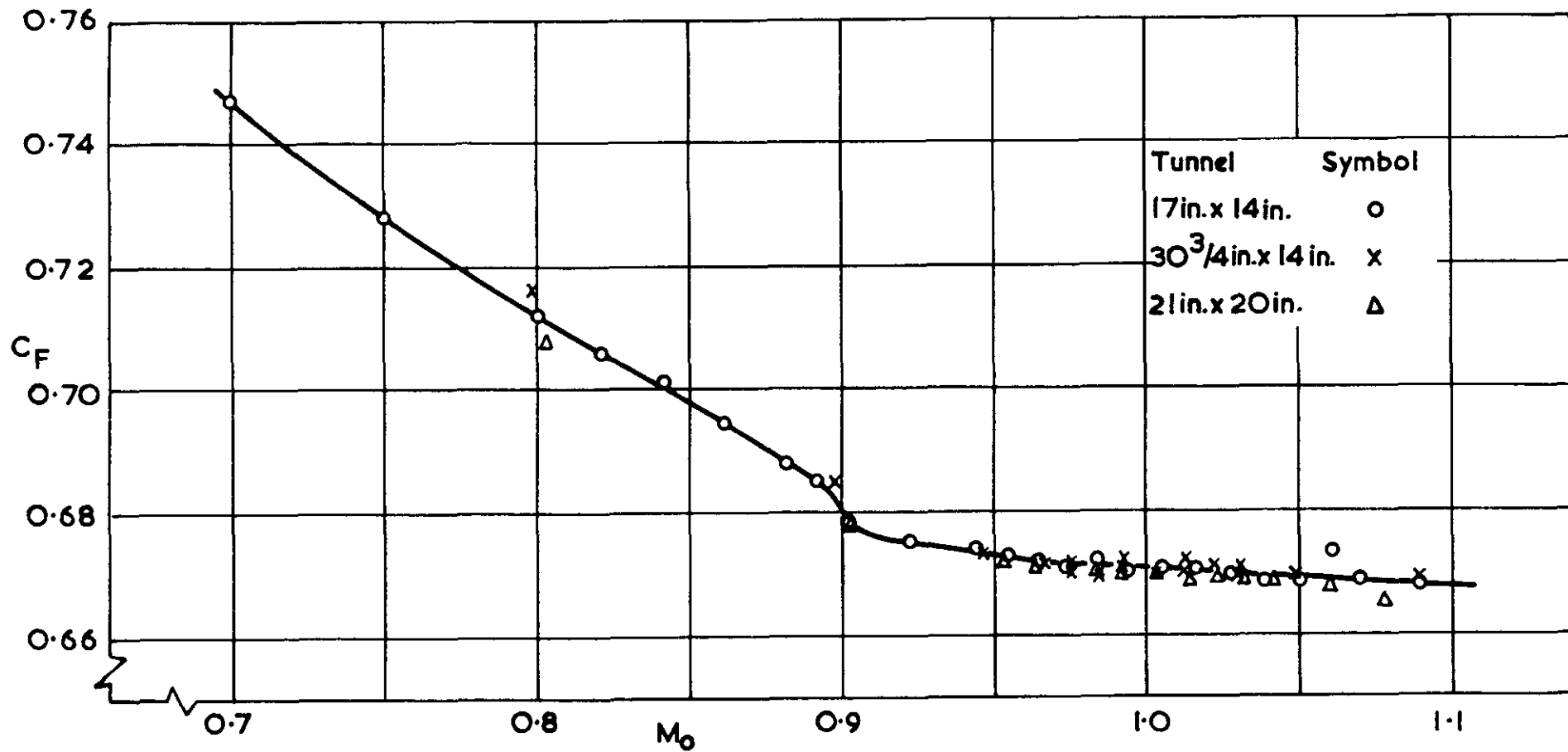
The variation of axial force with Mach number.

FIG. 15.
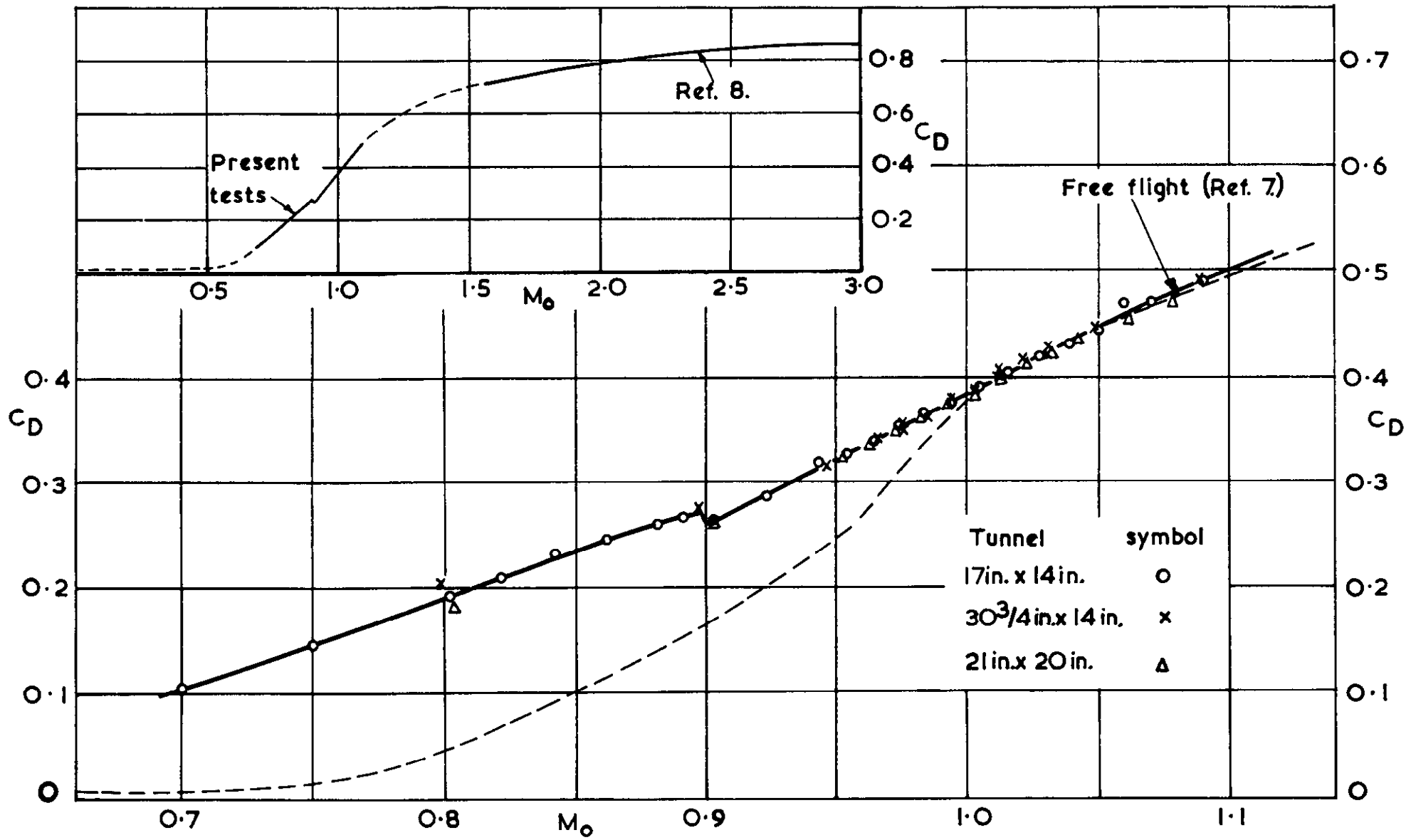
The variation of the nose drag coefficient with Mach number.

FIG. 16.